University of Cape Town

MAM5001W

Thesis presented for MSc Applied Mathematics

K-Complexity and the Jordan-Wigner transformation

Author:
Zayd Pandit [a]

Supervisors:
Prof J. Murugan [a,b]
Dr H.J.R. van Zyl [a,b]

[a] *Laboratory for Quantum Gravity & Strings, Department of Mathematics and Applied Mathematics, University of Cape Town, Cape Town, South Africa*
[b] *The National Institute for Theoretical and Computational Sciences, Private Bag X1, Matieland, South Africa*

March 27, 2025

Abstract

Krylov complexity is a measure of operator growth that demonstrates universal properties and bounds a large class of complexities. One such measure from this bounded class is operator size. The relationship between operator size and operator growth has been conjectured to be non-trivial due to the existence of duality transformations such as the Jordan-Wigner (JW) transformation which map small operators to large, non-local operators. We investigate this claim directly in the case of the JW transformation which maps the XY Heisenberg chain to the Kitaev chain. We numerically calculate the complexity of dual operators, and analyse the early and late time behaviour and symmetries. We find that for Open Boundary Conditions (OBC) the early time behaviour of the K-Complexity correlates with operator size, but that large operators can have very low K-Complexity if dual to a small operator. We find that for Periodic Boundary Conditions (PBC) larger operators produce larger early time growth, but do not correlate to larger late-time complexity regardless of the size of the dual operator. The difference between the OBC and PBC results arise from an often overlooked break in translational symmetry across the PBC Jordan-Wigner transformation. We also find that state complexity is not sensitive to the break in translational symmetry.

Contents

Acknowledgments

I would like to thank Dr van Zyl for his incredible generosity in his capacity as co-supervisor, and for being the nicest person ever. I have knocked on his door for a chat on average at least 3 times per week throughout the academic term for the past 2 years. I have no idea how he puts up with me. I am indebted to Professor Murugan for the incredible guidance and for always providing amazing academic and personal counsel. I would also like to thank Cameron Beetar for all the honest and insightful conversations about everything from complexity to trains.

I wish to thank Joshua Browne and Cole Faraday for allowing me to work in their offices when my brain stops functioning in my own office. Their company has been invaluable to me. Thank you to the UCT masters students for all the amazing lunchtime discussions, late-night office banter, hikes, and rock climbing trips. I've learnt and evolved so much personally through the experiences we've shared. I would also like to take this opportunity to apologize to the rest of my friends for the non-stop complaining about how work is going.

Thank you to my family whose support and patience has been unwavering, through all our ups and downs.

Lastly, a thank you to the National Research Foundation (NRF) for their generous sponsorship. Computations in this thesis were performed using facilities provided by the University of Cape Town's ICTS High Performance Computing team.

1 Overview and Motivation

Quantum many-body physics has emerged at the forefront of studying technologies that many believe will shape the future [1–3]. To me, however, its profound significance lies not just in its application to practical innovation but in the foundational role it plays in deepening our understanding of emergent phenomena. The field aims to understand fundamental phenomena in regimes where full knowledge of the system would be practically uncomputable. These phenomena include exotic states of matter, phase transitions, and entanglement—phenomena I find difficult to not think of as magical. But then again, what is magic but new physics?

Analysis of many-body systems often necessitates a numerical approach, as few are analytically tractable. One class of techniques are Krylov subspace methods; these are an extremely useful class of iterative numerical algorithms for finding approximate solutions to high-dimensional linear algebra problems [4–7]. These methods find their utility in being able to describe solutions without needing to manipulate the high-dimensional input directly. This is achieved by projecting the high-dimensional problem onto a lower dimensional Krylov subspace. These methods then tackle the problem within the Krylov subspace, which has a number of useful properties. The efficiency advantages over direct methods become even more pronounced when dealing with more structured or sparse matrix inputs [5, 8, 9].

In quantum many-body systems Hilbert space dimension often scales exponentially with system size. Modelling time-evolution then, often mandates efficient approximations and representations of the dynamics. For this reason the techniques of Krylov subspace methods have for decades been applied to the field of quantum and classical many-body systems, where it is often called the Recursion method [10].

The Krylov subspace methods are particularly suited to the task of approximating the dynamics of quantum many-body systems; in fact they construct a minimal subspace for a description of the dynamics. Here we can map the unitary time-evolution of a quantum state to the time-evolution of a particle hopping along a one-dimensional space, known as the Krylov chain [10–13]. By providing an efficient framework for understanding quantum dynamics, Krylov subspace methods offers a means for exploring deeper aspects of quantum systems, including quantum chaos.

The study of quantum chaos took off after the BGS conjecture suggested that the spectral statistics of quantum chaotic systems are described by random matrix theory (RMT) [14]. The consequence of which is that the behaviour of energy levels in a chaotic quantum system are universal—they are not governed by the system's Hamiltonian, but by RMT [15]. This notion of universality is foundational in the study of chaotic systems [16]. Building upon this, progress has been made linking quantum chaos to properties of ergodicity and thermalization [17, 18]. This led to connections with the Eigenstate Thermalization Hypothesis (ETH) [19–21] and the development of diagnostic tools such as the spectral form factor (SFF) [22, 23] and out-of-time-ordered correlators (OTOCs) [24]. In 2016 a quantum analog of the Lyapanov exponent was established using the out-of-order-correlators (OTOCs) and a universal bound on chaos was put forward. This was the so-called MSS

bound—a bound on the growth exponent of the OTOC which is saturated by maximally chaotic systems [25]. Although this result had limitations, it was clear at this point that the study of operator dynamics was key, and that its potential was not yet fully exploited.

The seminal work of Parker *et al.* [26] brought these ideas together. The work [26] reframed operator growth using Krylov subspace methods—establishing the notion of Krylov complexity (or K-complexity). K-complexity is indeed a unique measure of operator growth. They showed that it bounds from above an important class of observables. This class of observables includes the OTOC and complexity measures such as operator size. This work [26] formulated a rigorous relationship between K-complexity and the chaotic properties of quantum systems. For large N, infinite temperature systems, Lanczos coefficients grow at most linearly and K-complexity can grow at most exponentially, with the former being a stronger condition that implies the latter. Furthermore, this bound on the growth of K-complexity is saturated and reduces to the MSS bound when studying maximally chaotic systems [27].

The sensitivity of K-complexity to quantum chaos sparked an immediate interest in applications to holography. This excitement was due to indications that quantum gravity exhibits chaotic properties and that black holes are nature's fastest information scramblers [28]. Proposals were developed wherein operator growth is linked to wormhole growth under the holographic dictionary [29, 30]. However, the applications of K-Complexity as a probe of chaos have shown limitations; there exists counterexamples to the operator growth hypothesis for field theories [27, 31]. More precisely, free field theories and rational 2D CFTs exhibit the same Krylov growth exponent as maximally chaotic holographic CFTs. This however does not break the link between K-complexity and scrambling in general—the finite temperature growth exponent of K-complexity is bounded below by the growth of the OTOC, and bounded above by the MSS bound. The Krylov growth exponent is thus a tighter bound for scrambling than the MSS bound [27].

The swell of attention has sparked plenty of developments and generalizations of K-complexity in condensed-matter settings. This includes major developments in its application to open quantum systems. The first of these showed that Krylov complexity is suppressed by dissipation, and that its saturates at a finite value much smaller than that of a closed system with an equivalent Hamiltonian [32]. K-complexity has also been developed as a diagnostic in topological phase transitions [33], and recent progress has shown its applicability as an order parameter for chaotic-integrable transitions [34].

Of particular interest in this work, is the application of K-complexity to many-body systems, and understanding how K-complexity behaves across duality transformations[1]. Understanding how operators grow in dual theories is an important question which remains open. In high-energy physics, dualities such as AdS/CFT correspondence reveal deep connections between gauge theories and gravity, while in condensed matter settings, dualities such as particle-vortex duality and bosonization are crucial for understanding quantum critical points and phases of quantum matter [35]. As we have established, in isolated systems

[1]Duality transformations here refers to maps between different systems with the same physical degrees of freedom. This includes Gauge/Gravity duality, Bosonization, and T-duality. [35]

operator growth plays a key role in understanding of various phenomena such as chaos and thermalization. Understanding the commonalities between operator growth in dual theories could pave the way for applying operator growth and associated complexity metrics across the duality web [35–39].

A key feature of dual theories is that a local operator of one theory often maps to a non-local operator in the dual theory. Understanding the way operator growth compares across duality thus has a simple, but crucial component: how operator growth is affected by operator size[2].

The focus of our investigation is to examine the K-complexity of operators which are dual under a transformation that maps local to non-local operators. This directly attacks the connection between operator size and operator growth. Operator size and operator growth are distinct but related quantities; Parker *et al.* showed that the latter bounds the former from above. In that same work the authors provide an example of the Jordan-Wigner duality making it possible for operators to have large size and low complexity, saying:

> "In finite-dimensional systems, complexity should be a distinct concept from operator size. For instance, long Pauli strings generated in the non-interacting Ising models have nonetheless low complexity, since they can be transformed to simple fewbody operators under the Jordan-Wigner transform."

This statement can be extended into the following hypothesis:

> "Large (non-local) operators which can be mapped to small (local) operators via a duality transformation will exhibit similar K-Complexity to that of small (local) operators."

We would like to address the claim directly by investigating the critical and clear example that the Jordan-Wigner transformation provides. The Jordan-Wigner transformation relates the dual systems of the Transverse field Ising Model (TFIM) and Kitaev chain—systems that have been extensively studied in the complexity literature. This provides us with a finite dimensional playground and an expanse of literature to benchmark our results against [26, 40–43]. In particular, we will focus on two features of the K-Complexity: initial growth and the saturation value. We will assess these features' dependency on operator size, operator type and the boundary conditions imposed.

[2]Operator size can generally be defined as a measure of the spatial extent over which an operator acts. For instance consider the context of a spin-1/2 model. Here in the basis of Pauli matrices (with identity) we can define the operator size as measuring the number of non-identity operators present.

2 An introduction to K-Complexity

2.1 Complexity from scratch

Inspiration for the study of quantum complexity is derived from the field of algorithmic information theory, in particular the notion of Kolmogorov complexity [44]. The Kolmogorov complexity of an object is the length of the shortest computer program that can produce the object as output [45, 46]. The intuitive idea behind this is to classify objects according the number of components that are needed to assemble it. Similarly, quantum complexity aims to establish a measure of how difficult it is to get from one particular quantum state to another, using a set of predefined allowed unitary operations [47]. This leaves a clear detail to pin down—what should be chosen as the basis, the pre-defined set of operations, the building blocks to count?

One simple definition is that of circuit complexity [48, 49]. Here we simply define the complexity of an operator as the minimum number of elementary gates from a universal gate set needed to construct the operator. A drawback of this method is the dependence on the choice of gate set. Its universal practicality is limited by the minimization step often being computationally infeasible, and its lack of applicability to continuum theories.

A successful geometric continuation is Nielsen's approach [48, 50–52]. Here the complexity between two quantum states (a target and reference state) is described by the geodesic distance between their points on the corresponding manifold of states. To compute this complexity we need to specify target and reference states as well as a set of unitary gates, and an associated cost functional [53].

An alternative and natural approach in the context of quantum dynamics would be to measure the 'spread' or 'growth' of the operator or state across a chosen basis. The expectation being that more 'complex' dynamics are reflected in a larger spread across the relevant Hilbert space. This meshes nicely with the idea of chaotic dynamics producing quick 'filling up' of the Hilbert space. Such a measure would interpret the initial operator or state as the reference state and the time-evolved operator or state as the target state. This measure requires a choice of basis, and will surely depend heavily on this choice. Since the physics is unaffected by the basis choice, we are free to choose a convenient, uniquely defined one. Taking inspiration from Kolmogorov, Balasubramanian *et al.* showed that we can define a complexity of this type, namely spread complexity by minimizing a cost function over all possible choice of bases, and that this minimum is unique [54]. In Section 2.3 we follow the same approach for operator growth, we minimize over possible bases and show that the Krylov basis is the unique basis achieving this minimum at early times. Operator growth in the Krylov basis, also known as Krylov complexity or K-complexity [26, 33] is the key complexity relevant to this work. We will also include comparisons to state Krylov complexity, or spread complexity, which measures the spread of states in the Krylov basis [54].

2.2 Operator Growth

We will start off with some quantum Hamiltonian H and a time-dependent Heisenberg operator $\mathcal{O}(t)$ in the model. The evolution of the operator is given by the Heisenberg

equation of motion,

$$\partial_t \mathcal{O}(t) \;=\; i[H, \mathcal{O}(t)] \;= i\mathcal{L}\mathcal{O}(t)\;, \tag{2.1}$$

where $\mathcal{L} = [H, \cdot]$ is the Liouvillian superoperator. The solution to which is given by

$$\mathcal{O}(t) = e^{iHt}\mathcal{O}(0)e^{-iHt} \tag{2.2}$$

$$= e^{i\mathcal{L}t}\mathcal{O} \tag{2.3}$$

$$= \sum_{n=0}^{\infty} \frac{(it)^n}{n!}\mathcal{L}^n\mathcal{O} \tag{2.4}$$

where we've used Baker-Campbell-Hausdorff, Taylor expanded, and defined $\mathcal{O} \equiv \mathcal{O}(0)$.

With no inner product naturally defined, the space of operators is a complex vector space. We can upgrade it to a Hilbert space by equipping it with our choice of inner product, thus introducing a notion of distance between operators. We will use the infinite temperature Wightman inner product, also known as the Frobenius inner product [26],

$$(A|B) = \mathrm{Tr}(A^\dagger B)\;. \tag{2.5}$$

The choice of inner product introduces some freedom, and alternative inner products can be used to incorporate finite temperature, as we will briefly discuss in Appendix E.

Now, armed with our operator Hilbert space in hand, it is time to define what is meant by the 'spread' of an operator through the operator space. This we can do by defining a cost function which measures the overlap of the time-evolved reference operator with a particular basis, with each basis element assigned a particular weight. Specifically, we will consider a cost function with an ordered basis $\mathcal{B} = \{|B_n) : n = 0, 1, \ldots\}$ and the weight assigned being a positive increasing real sequence c_n,

$$C_{\mathcal{B}}(t) = \sum_n c_n |(\mathcal{O}(t)|B_n)|^2 \equiv \sum_n c_n |\phi_{\mathcal{B}}(n,t)|^2 \;=\; \sum_n c_n P_{\mathcal{B}}(n,t)\;. \tag{2.6}$$

Note that $|\phi_{\mathcal{B}}(n,t)|^2$ represents the probability for $\mathcal{O}(t)$ to be in the n'th basis vector[3] at time t. The positive increasing sequence c_n ensures a higher cost for further spread across the ordered basis.

This cost function is a quantity which strongly depends on the choice of basis. A natural choice would be to choose the basis which gives the minimum cost for all bases $\mathcal{B}$,

$$C(t) \;=\; \min_{\mathcal{B}} C_{\mathcal{B}}(t)\;. \tag{2.7}$$

We will show that if we proceed with a functional minimization, we will find that the Krylov basis minimizes the cost function for early times—and that this minimum is unique. We will do so following the technique in [54], where it was proven for spread (state) complexity.

[3] As is the case here, we will occasionally refer to operators as vectors of the relevant operator Hilbert space.

2.3 The Krylov basis minimizes the cost function

Theorem 1 *For any basis $\mathcal{B}$ and a positive real weight sequence c_n, the cost function $C_{\mathcal{B}}(t) = \sum_n c_n |(\mathcal{O}(t)|B_n)|^2$ minimizes for a complete Krylov basis $\mathcal{K}$ around $t = 0$.*

First, what is a complete Krylov basis? The operators $\tilde{\mathcal{O}}_n := \mathcal{L}^n\mathcal{O}$, for some operator $\mathcal{O}$, span the so-called *Krylov space*—a particular subspace of the Hilbert space. These operators are in general not mutually orthogonal. By orthogonalizing this spanning set we arrive at an orthonormal basis, $\mathcal{K} = \{|K_i) : i = 0, 1, 2 \ldots\}$, called the *Krylov basis*.

To prove the theorem we will work with the Taylor expansion of the cost functions near $t = 0$, and compare them order by order. Suppose we have two cost functions $C_{\mathcal{B}_1}(t)$ and $C_{\mathcal{B}_2}(t)$ for bases $\mathcal{B}_1$ and $\mathcal{B}_2$, each with a Taylor expansion convergent on the domain $0 \leq t \leq T$. We can then show that $C_{\mathcal{B}_1}(t) < C_{\mathcal{B}_2}(t)$ for $0 \leq t < T$, if for some k we have that $C^{(m)}_{\mathcal{B}_1} = C^{(m)}_{\mathcal{B}_2}$ for $m < k$, and $C^{(m)}_{\mathcal{B}_1} < C^{(m)}_{\mathcal{B}_2}$ for $m = k$, where here we've denoted $C^{(m)}_{\mathcal{B}} = d^m C_{\mathcal{B}}(t)/dt^m|_{t=0}$.

Thus, to prove Theorem 1 it is sufficient to show that for any basis $\mathcal{B}$, there exists k such that $C^{(m)}_{\mathcal{K}} = C^{(m)}_{\mathcal{B}}$ for $m < k$, and $C^{(m)}_{\mathcal{K}} \leq C^{(m)}_{\mathcal{B}}$ for $m = k$, with equality only if $\mathcal{B} = \mathcal{K}$. We will do so by using induction on the first N elements of $\mathcal{B}$.

Proof:

Base case: We know that $|K_0) = |\mathcal{O}(0))$. Suppose that $|\mathcal{B}_0) = |K_0)$. Then

$$C_{\mathcal{B}}(0) \;=\; \sum_n c_n |(\mathcal{O}(0)|B_n)|^2 \;=\; c_0 \,. \tag{2.8}$$

A basis that has $O(0)$ as its first element will have a lower complexity than those which do not. The latter would require bases of larger n to support the initial operator, which would be accompanied by a higher weight factor c_n.

Inductive step: We can express our time derivatives of the cost function in terms of the action of the Liouvillian. More specifically we will work with the derivatives of the probability amplitudes as

$$P^{(m)}_{\mathcal{B}}(n,t) = \frac{d^m}{dt^m}|(\mathcal{O}(t)|B_n)|^2 \tag{2.9}$$

$$= i^m \sum_{k=0}^{m} \binom{m}{k} (-1)^k (\mathcal{O}(t)|\mathcal{L}^{m-k}|B_n)(B_n|\mathcal{L}^k|\mathcal{O}(t)) \,, \tag{2.10}$$

where we've applied product rule and replaced the derivatives using Equation 2.1. We now write down a lemma which will get us most of the way through the proof.

Lemma 1 *Suppose $|B_i) = |K_i)$ up to phase for $i = 0, 1, \ldots, N-1$. Then $C^{(2N)}_{\mathcal{B}}(0) \geq C^{(2N)}_{\mathcal{K}}(0)$, with equality in the case that either $|\mathcal{K}| = N$ and $\mathcal{B}$ is a complete Krylov basis, or the case that $|B_N) = |K_N)$ up to a phase.*

Proof: Let us first consider the case where $n \geq N$ and $0 \leq m < 2N$ —here we will show that $P^{(m)}_{\mathcal{B}}(n, 0) = 0$. For $k < N$, $|B_k) = |K_k)$, and thus $\mathcal{L}^k|\mathcal{O})$ is a linear combination of $|B_0), \ldots, |B_{N-1})$. We then know that $(B_n|\mathcal{L}^k|\mathcal{O}) = 0$ for $k < N$ by the orthogonality of

$\mathcal{B}$. Now for $m < 2N$, we must have that either $k < N$ or $m - k < N$. Recall the form of $P_{\mathcal{B}}^{(m)}(n,0)$ in Equation 2.10 where every term contains $(\mathcal{O}(t)|\mathcal{L}^{m-k}|B_n)(B_n|\mathcal{L}^k|\mathcal{O}(t))$. Thus, every term in the sum is zero, and we have that

$$P_{\mathcal{B}}^{(m)}(n,0) = 0 \,, \qquad \text{for } n \geq N,\ m < 2N \,. \tag{2.11}$$

Now we shall consider the case where $n \geq N$ and $m = 2N$. Here there will be a single non-zero term in the expansion of $P_{\mathcal{B}}^{(n)}(n,0)$,

$$P_{\mathcal{B}}^{(2N)}(n,0) = \binom{2N}{N}(\mathcal{O}|\mathcal{L}^N|B_n)(B_n|\mathcal{L}^N|\mathcal{O}) \,, \qquad \text{for } n \geq N,\ m = 2N \,. \tag{2.12}$$

We need one last construction to tease out the difference between the Krylov basis and all other basis choices in the expression above. Consider some basis operator $|\tilde{K}_N) \propto |K_N)$. By the definition of the Krylov basis, $|\tilde{K}_N)$ is the component of $\mathcal{L}^N|\mathcal{O})$ that is orthogonal to $|K_0) \ldots, |K_{N-1})$, and by assumption orthogonal to $|B_0), \ldots, |B_{N-1})$.

Following from 2.12 we have that for $n \geq N$,

$$P_{\mathcal{B}}^{(2N)}(n,0) \;=\; \binom{2N}{N}(\tilde{K}_N|B_n)(B_n|\tilde{K}_N) \,. \tag{2.13}$$

This is because the component of $\mathcal{L}^N|\mathcal{O})$ that is parallel to $|B_0), \ldots, |B_{N-1})$ must be orthogonal to $|B_N)$, so only the perpendicular component of $L^N|\mathcal{O})$, $|\tilde{K}_N)$, remains.

Note that if $|\tilde{K}_N) = 0$, then $|\mathcal{K}| = N$, and $\mathcal{B}$ would simply be a complete Krylov basis. In this case $C_{\mathcal{B}}^{(2N)}(0) = C_{\mathcal{K}}^{(2N)}(0)$ and we arrive at the first equality case of our lemma. If on the other hand $(\tilde{K}_N|\tilde{K}_N) > 0$, then we have that,

$$C_{\mathcal{B}}^{(2N)}(0) \;=\; \sum_n c_n P_{\mathcal{B}}^{(2N)}(n,0) \tag{2.14}$$

$$\;=\; \sum_n^{N-1} c_n P_{\mathcal{B}}^{(2N)}(n,0) + \binom{2N}{N} \sum_{n=N}^{D} c_n (\tilde{K}_N|B_n)(B_n|\tilde{K}_N) \,, \tag{2.15}$$

where D is the full Hilbert space dimension. If we consider Equation 2.15 for the Krylov basis $\mathcal{K}$, the last term simplifies since $|\tilde{K}_N)$ is orthogonal to all $|K_n)$ for $n > N$:

$$C_{\mathcal{K}}^{(2N)}(0) \;=\; \sum_n^{N-1} c_n P_{\mathcal{K}}^{(2N)}(n,0) + \binom{2N}{N} \sum_{n=N}^{D} c_n (\tilde{K}_N|\tilde{K}_N) \,. \tag{2.16}$$

Finally, we note that since c_n is increasing, we must have that

$$C_{\mathcal{B}}^{(2N)}(0) \;\leq\; C_{\mathcal{K}}^{(2N)}(0) \,, \tag{2.17}$$

with equality only if it is the case that $|B_n) \propto |\tilde{K}_N)$ up to a phase. This completes the proof of the lemma.

Let us continue with the proof of Theorem 1. We now know from Equation 2.11 that $P_{\mathcal{B}}^{(m)}(n,0) = 0$, for $n \geq N$ and $m < 2N$. This means that the first $2N$ derivatives of $C_{\mathcal{B}}(t)$ equals that of $C_{\mathcal{K}}(t)$, since the rest of the probability amplitudes are zero. We also know

from Lemma 1 that since the $2N$'th derivative of $C_{\mathcal{B}}(t)$ will be larger than that of $C_{\mathcal{K}}(t)$, unless $\mathcal{B}$ is equal to a complete Krylov basis up to a phase, in which case the cost functions are equal. Thus, $C_{\mathcal{B}}(t) \geq C_{\mathcal{K}}(t)$, with equality when $\mathcal{B} = \mathcal{K}$ is up to a phase.

We have shown that for any basis $\mathcal{B}$ there must exist some k such that $C_{\mathcal{B}}^{(m)} = C_{\mathcal{K}}^{(m)}$ for $m < k$ and $C_{\mathcal{B}}^{(m)} \geq C_{\mathcal{K}}^{(m)}$ for $m = k$, with equality if $\mathcal{B} = \mathcal{K}$. This completes the proof of Theorem 1.

2.4 Operator Growth in the Krylov basis

As described before, by orthogonalizing the spanning set of the Krylov subspace of an operator $\{\mathcal{O}, \mathcal{L}\mathcal{O}, \mathcal{L}^2\mathcal{O}, \ldots\}$, we can produce a Krylov basis $\mathcal{K} = \{|K_i) : i = 0, 1, 2 \ldots\}$. As we have shown, this is the unique basis which minimizes cost functions of the form given in Equation 2.6.

The orthogonalization can be done through a Gram-Schmidt type procedure. Most convenient for us would be to produce the Krylov basis recursively using the *Lanczos algorithm*[4] [5]. From the Lanczos algorithm we can extract Lanczos coefficients which are generated as norms during the orthogonalization. The Lanczos coefficients encode all the dynamic information we would wish to extract from the evolution in the Krylov space [6].

In the Krylov basis the Liouvillian takes on a tri-diagonal form

$$\mathcal{L}|K_n) = b_n|K_{n-1}) + b_{n+1}|K_{n+1}) + a_n|K_n) \ , \tag{2.18}$$

where $|K_n)$ are the Krylov basis operators, and a_n and b_n are the Lanczos coefficients. We can see that the diagonal entries will be zero if H and $\mathcal{O}$ are Hermitian. For this reason the diagonal term is often neglected in the literature.

We would like to describe the evolution of an operator in terms of its spread along the Krylov basis. Simply expanding some time-evolved operator in terms of the Krylov-basis we get

$$|\mathcal{O}(t)) \ = \ \sum_n \phi_n(t)|K_n) \ , \tag{2.19}$$

and its time derivative

$$\partial_t|\mathcal{O}(t)) \ = \ \sum_n \partial_t\phi_n(t)|K_n) \ , \tag{2.20}$$

where Equation 2.19 defines ϕ_n, the probability amplitudes. Note that as before, but with different notation, $|\phi_n(t)|^2$ describes the probability of the operator being in the n'th Krylov basis vector at time t. We can also write the time derivative of the time-evolved operator in the Krylov basis by using Equations 2.18 and 2.1:

$$\partial_t|\mathcal{O}(t)) \ = \ \sum_n \phi_n(t)\Big(b_n|K_{n-1}) + b_{n+1}|K_{n+1}) + a_n|K_n)\Big) \ . \tag{2.21}$$

Finally, using Equations 2.20 and 2.21 we get an expression for the evolution of the probability amplitudes in terms of the Lanczos coefficients:

$$i\partial_t\phi_n(t) \ = \ b_n\phi_{n-1}(t) + b_{n+1}\phi_{n+1}(t) + a_n\phi_n(t) \ . \tag{2.22}$$

[4] See Section 6.1 for the algorithm outline and implementation details.

[5] Another common means of obtaining Lanczos coefficients is via the so-called *Moments method*, which uses the moments of the return amplitude, $C(t) = (\mathcal{O}|e^{it\mathcal{L}}|\mathcal{O})$, also known as the autocorrleation function

[6] In [26], the authors present five equivalent representations for encoding operator dynamics: the autocorrelation function $C(t) = \phi_0(t) = (\mathcal{O}|e^{it\mathcal{L}}|\mathcal{O})$, the spectral function, $\Phi(\omega) = \int_{-\infty}^{\infty} C(t)e^{-i\omega t}dt$, the Green's function, $G(z) = \left(\mathcal{O}|\frac{1}{z-\mathcal{L}}|\mathcal{O}\right) = i\int_0^{\infty} e^{-izt}C(t)dt$, the autocorrelation function moments $\mu_{2n} \coloneqq (\mathcal{O}|\mathcal{L}^{2n}|\mathcal{O}) = \frac{d^{2n}}{dt^{2n}}C(t)|_{t=0}$, and lastly, the Lanczos coefficients $\{a_n\}$ and $\{b_n\}$. The non-linear link between the Lanczos coefficients and the other four representations is presented in the Appendix of [26]. Since all five are equivalent, we choose between them based on convenience.

This is a discrete Schrödinger equation which conserves probability, i.e. $\sum_n |\phi_n(t)|^2 = 1$. With knowledge of the Lanczos coefficients a_n and b_n, this equation allows us to solve for the time-evolved probability amplitudes, $\phi_n(t)$, using the initial condition $\phi_n(0) = \delta_{n,0}$.

2.5 Defining K-Complexity

With Equation 2.19 we wrote the evolution of an operator in terms of evolution along the Krylov basis. This evolution along the chain of operators K_n, the *Krylov Chain*, is governed by the evolution of the probability amplitudes ϕ_n in Equation 2.22. A very natural way to measure the spread of the operator along the Krylov basis would thus be

$$K(t) \equiv \sum_n n|\phi_n(t)|^2 \,. \tag{2.23}$$

Rewriting as an expectation value of the time-evolved operator:

$$K(t) = (\mathcal{O}(t)|\hat{K}|\mathcal{O}(t)) \,, \tag{2.24}$$

where we have the *Krylov Complexity Operator*

$$\hat{K} = \sum_n n|K_n)(K_n| \,. \tag{2.25}$$

$K(t)$ takes the form of the cost functions in Equation 2.6 where $c_n = n$. The positive definite weight factor n assigns 'higher cost' to states which require support further along the chain of Krylov basis elements. Furthermore, we can see that K-Complexity has the interpretation of being the average position of the operator along the Krylov Chain. With this definition, the hope is that this first moment of the distribution of ϕ_n's captures important dynamical information relevant for specific tasks. As discussed previously these tasks include diagnosis of chaotic behaviour and the detection of phase transitions.

2.6 Krylov complexity bounds Q-complexities from above

We can ground the idea of K-complexity by establishing a relationship between it and similar, more familiar quantities. Parker *et al.* [26] demonstrated that for a particular class of observables, termed "Q-complexities", the growth of any Q-complexity is bounded above by K-Complexity. The class includes familiar observables such as operator size and the out-of-time-ordered correlator (OTOC), as we will show in Sections 3.1 and B.1, respectively. The original proof applied to the context of operator complexities, but as seen in [55], it can be extended to a more general Hilbert space. This allows state complexity to be included. In the following, we present a version of the extended result with a bit more detail in the proof.

We shall first define the Q-complexity of a given time-evolved reference state, $\mathcal{O}(t) \in \mathcal{H}$, to be given by the expectation value

$$Q(t) = \Big(\mathcal{O}(t)|\hat{Q}|\mathcal{O}(t)\Big) \tag{2.26}$$

where $\hat{Q}$ is some hermitian operator. Now we impose three simple properties on $\hat{Q}$ that define it to be of the class of Q-complexities:

1. $\hat{Q}$ is positive semi-definite. This ensures that the q-complexity is always greater than or equal to zero. Suppose that the n'th eigenstate of $\hat{Q}$ is given by $|q_n)$ with associated eigenvalue q_n, then
$$\hat{Q} = \sum_a q_a |q_a)(q_a| \,, \qquad q_a \geq 0 \,. \tag{2.27}$$

2. Q-complexity cannot change significantly under a single application of the Liouvillian and the initial operator has a low Q-complexity. This is satisfied if there exists a positive constant M such that:

   (a) It holds that
   $$|q_a - q_b| > M \implies (q_a|\mathcal{L}|q_b) = 0 \tag{2.28}$$

   (b) and, for the same M, we have
   $$|q_a| > M \implies (q_a|\mathcal{O}) = 0 \,. \tag{2.29}$$

K-Complexity is naturally an element of the Q-complexity family. The K-Complexity operator is given by $\hat{K} = \sum_n n|K_n)(K_n|$, where $|K_n)$ are the Krylov basis elements. We have also chosen to have the positive definite basis weighting of n; this corresponds to q-values $q_n = n$. Note that the Krylov basis has some properties which make it notably unique in the q-complexity class. The action of the Liouvillian, $\mathcal{L}$, acts as a nearest-neighbour spread on the Krylov chain, as we have seen in Equation 2.18. This means that the resulting K-complexity can change by at most 1 with a single application of $\mathcal{L}$. This leads us to intuit that the eigenbases for any other Q-operator must be more 'dilated', or 'spread out' than the Krylov basis. In other words, applications of the Liouvillian count through the Krylov basis faster than any other eigenbasis of a Q-operator. The dilation effect, which we will show in Lemma 2, implies that any $Q(t)$ will be bounded above by $K(t)$. We will now show this rigorously.

Theorem 2 *Given any Q-complexity, $Q(t)$, the K-Complexity, $K(t)$, and some constant $M > 0$,*
$$Q(t) \leq MK(t) \,.$$

Proof:

We will start off with a lemma which demonstrates the dilation of other Q-eigenbases relative to the Krylov basis.

Lemma 2 *For q-values where $q > M(n+1)$,*
$$(q|\mathcal{L}^n|\mathcal{O}) \;=\; 0 \,.$$

Proof:

We will show this by using induction on n. The base case $n = 0$ is true by assumption using Equation 2.29.

Now we assume that the Lemma holds for $n = \nu$. We thus have that $(q|\mathcal{L}^\nu|\mathcal{O}) = 0$ if $q > M(\nu+1)$. It then must be the case that the support of $\mathcal{L}^\nu|\mathcal{O})$ lies on the rest of the q-eigenstates, i.e. we must have that

$$\mathcal{L}^\nu|\mathcal{O}) \;=\; \sum_a c_a|q_a) \qquad \text{for} \qquad q_a \leq M(\nu+1)\;, \tag{2.30}$$

where c_a are some constant coefficients. We can now proceed with our inductive step with $n = \nu + 1$. First we expand our expectation value in terms of the q-eigenstates as

$$\begin{aligned}(q|\mathcal{L}^{\nu+1}|\mathcal{O}) \;&=\; (q|\mathcal{L}^\nu\mathcal{L}|\mathcal{O}) &(2.31)\\ &=\; \sum_{a\in\alpha} c_a(q|\mathcal{L}|q_a)\;, &(2.32)\end{aligned}$$

where $\alpha = \{a : q_a \leq M(\nu+1)\}$, and we've used our $n = \nu$ assumption. Now, if we have some q where $q > M((\nu+1)+1) = M\nu + 2M$ then we must have that $|q - q_a| > |M\nu + 2M - (M\nu + M)| = M$ for all $a \in \alpha$. Recall from the assumption 2.28 that $|q - q_a| > M \implies (q|\mathcal{L}|q_a) = 0$. Assembling the pieces laid out just above, we have that

$$q > M((\nu+1)+1) \implies \left(q|\mathcal{L}^{\nu+1}|\mathcal{O}\right) \;=\; 0\;. \tag{2.33}$$

Thus by induction we have proved the Lemma.

Now we shall bring our focus back to the surrounding theorem. Since each Krylov basis $|K_n)$ is a linear combination of $\mathcal{L}^m|\mathcal{O})$ for $m = \{0, \ldots, n\}$, from our Lemma we have a simple corollary that

$$q > M(n+1) \implies (q|K_n) = 0\;. \tag{2.34}$$

This tells us that for any fixed q, if n is strictly less that some critical value $n(q)$, then the Krylov basis $|K_n)$ must have zero overlap with the associated eigenvector $|q)$. From the corollary 2.34, we can see that we can use the value $n(q) = \frac{q}{m} - 1$.

Due to the Q-complexities properties 2.28 and 2.29, we know that the Q-complexities' eigenstates should overlap for q-values below some critical value associated with M. Combining this with corollary 2.34 then demonstrates the 'dilation' of the other Q-eigenbases relative to the Krylov basis.

We now need to introduce some new objects before we bring it all together. For some arbitrary state $|\Phi) \in \mathcal{H}$, we can re-write the expectation value of the Q operator as

$$\begin{aligned}(\Phi|\hat{Q}|\Phi) \;&=\; (\Phi|\sum_{a\geq 0} q_a|q_a)(q_a|\Phi) &(2.35)\\ &=\; \sum_{a\geq 0} q_a|(q_a|\Phi)|^2 &(2.36)\\ &\equiv\; \int_{\mathbb{R}^+} dq\, q\, \mathcal{P}(q) &(2.37)\end{aligned}$$

where in the last line we're defining a probability distribution function (PDF). We also require the cumulative distribution function (CDF),

$$\mathcal{C}(q) \;\coloneqq\; \int_q^{+\infty} ds\, \mathcal{P}(s)\;. \tag{2.38}$$

Now we have a useful property relating equations 2.37 and 2.38: [7]

$$\int_{\mathbb{R}^+} dq\, q\, \mathcal{P}(q) \;=\; \int_{\mathbb{R}^+} dq\, \mathcal{C}(q)\;. \tag{2.39}$$

We now define the projector onto the eigenspaces of Q with eigenvalues larger than or equal to q:

$$P^Q(q) \coloneqq \sum_{a, q_a \geq q} |q_a)(q_a|\;. \tag{2.40}$$

Similarly we can construct a projector onto the eigenspaces of K with eigenvalues larger than n,

$$P^K(n) \coloneqq \sum_{m \geq n} |K_m)(K_m|\;. \tag{2.41}$$

If we re-write the CDF in terms of the discrete form of the projectors as

$$\mathcal{C}(q) \;=\; \sum_{a, q_a \geq q} |(q_a|\Phi)|^2 = \left(\Phi|P^Q(q)|\Phi\right)\;, \tag{2.42}$$

and we then use the fact that integral of the CDF is the Q-complexity expectation value because Equations 2.39 and 2.37, then we can write the Q-complexity expectation value in terms of the expectation value of the projectors:

$$\left(\Phi|\hat{Q}|\Phi\right) \;=\; \int_{\mathbb{R}^+} dq\, \left(\Phi|P^Q(q)|\Phi\right)\;. \tag{2.43}$$

We can now use the corollary 2.34, which gave us a condition for the eigenbases overlap, to tell us about how the two projectors overlap. We can see that,

$$P^Q(q)(1 - P^K(n(q))) \;=\; \sum_{a, q_a \geq q} \sum_{m < n(q)} |q_a)(q_a|K_m)(K_m| \;=\; 0\;. \tag{2.44}$$

We can then see that multiplying by the $P^K(n(q))$ does nothing more than $P^Q(q)$. This is expressed as:

$$P^Q(q)P^K(n(q)) \;=\; P^Q(q)\;, \qquad \text{and} \qquad P^K(n(q))P^Q(q) \;=\; P^Q(q)\;. \tag{2.45}$$

Now we use this to relate the expectation values of the projectors,

$$\begin{aligned} \left(\Phi|P^Q(q)|\Phi\right) \;&=\; \left(\Phi|P^K(n(q))P^Q(q)P^K(n(q))|\Phi\right) && (2.46)\\ &\leq \left(\Phi|P^K(n(q))P^K(n(q)|\Phi)\right) && (2.47)\\ &= \left(\Phi|P^K(n(q))|\Phi)\right)\;. && (2.48) \end{aligned}$$

Finally, using Equations 2.43 and 2.48, we can write

$$\begin{aligned} \left(\Phi|\hat{Q}|\Phi\right) \;&=\; \int_{\mathbb{R}^+} dq\, \left(\Phi|P^Q(q)|\Phi\right) && (2.49)\\ &\leq \int_{\mathbb{R}^+} dq\, \left(\Phi|P^K(n(q))|\Phi\right)\;. && (2.50) \end{aligned}$$

[7] Proof of this property: $\int_{\mathbb{R}^+} dq\, \mathcal{C}(q) = \int_{\mathbb{R}^+} dq \int_q^{+\infty} ds\, \mathcal{P}(s) = \int_{\mathbb{R}^+} ds \int_0^s dq\, \mathcal{P}(s) = \int_{\mathbb{R}^+} ds\, s\, \mathcal{P}(s)$, where in the second equality we've re-expressed the integration region, which is possible since Fubini's theorem holds.

Changing the integration variable from q to n, we get a Jacobian factor $\left(\frac{dn}{dq}\big|_{q=q_n}\right)^{-1}$. We can now use the critical value from the Lemma corollary $n(q) = \frac{q}{M} - 1$, which sets the Jacobian factor to M. Thus, we have that

$$\left(\Phi|\hat{Q}|\Phi\right) \leq M \int_{\mathbb{R}^+} dn \left(\Phi|P^Q(n)|\Phi\right) = M \left(\Phi|\hat{K}|\Phi\right) . \tag{2.51}$$

For the case corresponding to the time-evolved reference state, $|\Phi) = |\mathcal{O}(t))$, we get

$$Q(t) \leq MK(t) , \tag{2.52}$$

which concludes our proof of Theorem 2. We have thus in this subchapter shown that Q-complexities are bounded above by K-complexity.

2.7 Geometric properties of K-complexity

Interestingly, we can associate a relatively simple geometric interpretation to operator growth. It is possible to construct a geometry for the space of coherent states of a quantum system using the Fubini-Study metric (or information metric). Caputa *et al.* showed that for some systems that Krylov complexity at some time t is exactly proportional to the volume enclosed by the geodesic radius $r = \alpha t$ [33].

Recently it was argued that Krylov complexity cannot be a measure of distance between states or operators due an apparent failure to satisfy triangle inequality [56]. More explicitly, if we consider the complexity of three states separated by time evolution, A, B, C, we will find that the difference in complexity between states A and C is not necessarily less than the sum of the difference in complexity between A and B and the difference in complexity between B and C. Although the above statement is true, we cannot draw from it the conclusion that Krylov complexity is not a measure of distance. Krylov complexity is a measure of distance defined using the reference state to construct the basis. The distance to some target state is only well-defined from a single point—the reference state which generated the Krylov basis. We can think of this as every state having its own distance measure from it to all other states accessible via time-evolution. In the example used above of three states separated by time-evolution, the complexity is measured using a common Krylov basis, say the basis of A. According to the definition of K-complexity outlined above, the complexity between A and B is well-defined as the K-complexity of B w.r.t reference state A, and similarly the K-complexity between A and C is the K-complexity C w.r.t A. However, the complexity difference between B and C using the Krylov basis of A cannot be granted this interpretation. In order to compare apples to apples, we can only compare distances that are measured from the unique reference operator that generated the Krylov basis.

2.8 Symmetries in K-Complexity

Symmetries present in the operator dynamics will significantly impact the behaviour of the K-complexity. When the operator evolution is restricted to a symmetry subspace its Krylov subspace will be smaller, as will be demonstrated. The Krylov subspace dimension bounds the K-complexity from above, and is correlated to the K-complexity saturation value for chaotic systems.

In this work, we are concerned exclusively with the case where the target operator is the time-evolved reference operator. The K-Complexity is then fully determined by the reference operator and the Hamiltonian. An important property of K-Complexity (and spread complexity) is that it is invariant under simultaneous unitary transformations of the reference operator (reference state) and the Hamiltonian:

$$K(t;|\mathcal{O}),H) \;=\; K(t;\,U|\mathcal{O}),\,UHU^\dagger)\;. \tag{2.53}$$

Suppose we have some unitary symmetry of the Hamiltonian, U, meaning that $U^\dagger U = 1$ and $U^\dagger HU = H$, and thus $[H,U] = 0$. If we now consider the same transformation applied to the reference operator (state),

$$|\mathcal{O}) \mapsto |\mathcal{O}') = U|\mathcal{O})\;, \tag{2.54}$$

applying the Lanczos algorithm, we arrive at some new transformed Krylov basis $\{|K'_n) : n = 1,\ldots,\mathcal{K}'_D\}$ with new Lanczos coefficients $\{a'_n\}$ and $\{b'_n\}$. Under this transformation, the Krylov dimension and the Lanczos coefficients are invariant, $\mathcal{K}'_D = \mathcal{K}_D$, $\{a'_n\} = \{a_n\}$ and $\{b'_n\} = \{b_n\}$, while the Krylov basis gets transformed as $|K_n) \mapsto U|K_n)$. We show this explicitly in the Appendix F.1.

We know that physical observables are invariant under the application of a constant shift to the Hamiltonian. It is thus imperative to know what the impact of a translation of the Hamiltonian will have on resulting complexity. We can write this translation as

$$H \mapsto H' = H - \alpha I\;, \tag{2.55}$$

where $\alpha \in \mathbb{R}$. By similar strong induction proof used in F.1, we can show that $\mathcal{K}_D$ is invariant, and $\forall n < \mathcal{K}_D$, b_n and $|K_n)$ are invariant while the a_n coefficients are translated $a_n \mapsto a_n - \alpha$.

Rescalings of the Hamiltonian affect the time-scale of the behaviour. We can define a constant rescaling transformation as

$$H \mapsto H' = \beta H\;, \tag{2.56}$$

where $\beta \in \mathbb{R}$. We can show by induction that $\mathcal{K}_D$ and $|K_n)$ are invariant, while the Lanczos coefficients get rescaled as $a_n \mapsto \beta a_n$ and $b_n \mapsto \beta b_n$, for $n < \mathcal{K}_D$.

3 Operator Size

Operator size can generally be defined as a measure of the spatial extent over which an operator acts. A simple way to quantify this is by counting the number of non-trivially acting simple operators that appear in a product expansion of the operator [57]. In the context of quantum chaos, "non-trivial" operators are typically considered to be non-identity operators, as chaotic systems tend to exhibit ergodic behavior for all non-identity operators, with only a few exceptions such as scar states [58].

3.1 Operator size is a Q-complexity

Following [55], we will use a system of N qudits as an illustrative example. The Hilbert space of N qudits is a tensor product of d-dimensional individual qudit spaces, resulting in a total dimension of $D = d^N$. The corresponding operator space will thus have dimension $D^2 = d^{2N}$. For some operator $\mathcal{O}$, represented as a tensor product of site-subspace operators, we can simply define the operator size of $\mathcal{O}$ as the number of sites upon which it acts non-trivially. If $\mathcal{O}$ is a linear combination of operators which each have a tensor product structure, the definition becomes more nuanced. In this case, we can define the operator size as the weighted average of the sizes of each individual tensor product operator within $\mathcal{O}$. Labelling the set of tensor-product operators as ρ, the associated Q-complexity for operator size can be written

$$Q(t) \;=\; \sum_{\rho} \text{size}(\rho) \;\; |(\rho|\mathcal{O}(t))|^2 \; . \tag{3.1}$$

All operators in ρ can be labelled as $= |s, j)$, where the first argument specifies the subspace of operators with size $s = 0, \ldots, N$, and j enumerates the operators in the subspace of fixed size s, which runs over $j = 1, \ldots, h(s)$. Here $h(s)$ is the number of linearly independent tensor-product operator chains for some fixed size s. The dimension of the operator space of a single qudit that excludes the identity operator is $d^2 - 1$; combining this on-site freedom with the number of site arrangements, we can express $h(s)$ as

$$h(s) \;=\; \binom{N}{s} \left(d^2 - 1\right)^s \; . \tag{3.2}$$

The explicit form of the associated Q operator is thus

$$\hat{Q}_{\text{size}} \;=\; \sum_{s=0}^{N} \; s \; \sum_{j=1}^{h(s)} |s, j)(s, j| \; . \tag{3.3}$$

The Q-complexity condition 2.27 is satisfied since the complexity eigenvalues, $s = 0, \ldots, N$, are positive semi-definite. Given a k-local Hamiltonian and an initial operator of size r, it follows that conditions 2.28 and 2.29 are satisfied by $M = \max(k, r)$. Thus, we conclude that the operator size complexity defined in Equation 3.3 is a Q-complexity.

3.2 Defining operator size

Put simply, the Q-complexity of operator size or 'Size complexity' is the probability distribution of the size of the time-evolved operator $\mathcal{O}(t)$ in a basis of operators which are organized by size. Operator size has an intuitive relationship to Krylov complexity. Consider a k-local Hamiltonian and an operator that is initially small. In the thermodynamic limit, the action of the Liouvillian on the operator must incrementally increase the operator size, and it must produce some projection of the operator onto new Krylov basis elements. Therefore, in this limit, we can expect operator size and K-complexity to display similar qualitative behaviour [55, 59, 60]. For finite size systems, operator size is bounded by the system's maximum spatial extent—such as N, in the case of the N-qudit chain. Meanwhile, K-complexity, with its completely non-degenerate eigenvalues, can grow well beyond the point at which operator size saturates.

Size complexity has been shown to measure the process of *scrambling* [57]. Scrambling refers to the process whereby localized information becomes distributed across the entire system, making information about the initial state inaccessible without knowledge of at least half of the degrees of freedom [28]. In chaotic systems, size complexity will grow exponentially up to the saturation time-scale, or scrambling time $t_s \sim \log N$ [59, 61]. In contrast, the K-complexity of finite chaotic systems can continue growing up to the Heisenberg time $t \sim e^N$ [55, 60].

Of particular concern for this work is the notion of operator size within the Transverse Field Ising Model (TFIM) system, where the Hilbert space is composed of a tensor product of two-dimensional spin-1/2 particle Hilbert spaces. As mentioned in the introduction, we define operator size in the TFIM system as the number of non-identity matrices in the operator's tensor product decomposition. This definition naturally qualifies as a Q-complexity measure and, as such, is bounded above by K-complexity.

We could consider an alternative definition of operator size tailored to the integrable system of the TFIM. In this case one might argue that an operator with alignment to the magnetic field at any given site would contribute less to the overall spread through the operator Hilbert space than one orthogonal to the magnetic field. Suppose the magnetic field were in the z-direction. We could then propose an alternative, TFIM specific, measure of size that counts the number of non-identity, non-σ^z operators present in the tensor product expansion. As our results will show, this definition appears to correlate more closely with early time operator growth in the TFIM than the standard measure of operator size.

4 Recursively generating probability amplitudes

We often work with large systems, or infinite dimensional systems. I'm sure this is not surprising, but nonetheless disappointing. In these cases it is often not possible to obtain a complete set of Lanczos coefficients, or complete Krylov basis. Naturally these incomplete sets will encode less dynamical information; it is thus important to track how the information loss affects the results. In this section we present a formalism for calculating K-Complexity which allows us to measure the error in the results and determine regions of validity. This is useful for large systems where the full set of Lanczos coefficients are not accessible, or where there is large uncertainty in the Lanczos coefficients. This technique was originally employed for determining approximate regions of validity in the Spread complexity of the Bateman oscillator [62].

4.1 The problem with the canonical method

The canonical approach to calculating K-Complexity is as follows: Calculate the Lanczos coefficients via a Lanczos Algorithm using the Hamiltonian, or via the Moments method using the autocorrelation function. Calculate the probability amplitudes, $\phi_n(t)$, via the Schrödinger equation 2.22. Then, using Equation 2.23, calculate the K-Complexity as the sum of the probability amplitudes with linear weighting n.

Consider the case where we only have access to an incomplete set of Lanczos coefficients, b_n, for $n = 1, \ldots, N$. In this case the Schrödinger equation 2.22 would contain a boundary condition that incorrectly sets the final probability amplitude, ϕ_{N+1} to zero, which corresponds to $b_{N+1} = 0$. This incorrect setting of the boundary will affect the solutions to the Schrödinger equation for all t, but there will be a timescale during which the solutions remain sufficiently accurate. Recall that the Schrödinger equation describes a complex diffusion process along the Krylov chain with an infinite information propagation speed. The initial condition is $\phi_n(0) = \delta_{n,0}$; at any time $t > 0$ the solutions, $\phi_n(t)$, will have non-zero support throughout the chain, including at the boundary $n = N$. Once the solutions $\phi_n(t)$ develop significant support at the $n = N$ boundary, their evolution will begin to be strongly affected by the incorrect boundary condition. It is at this time-scale that the K-complexity derived from the truncated set of Lanczos coefficients will significantly deviate from the true K-Complexity. There is, therefore, a time interval for which the solutions will be accurate up to some tolerance—but estimating this time-scale is generally difficult.

Consider a second case where we have obtained the full set of Lanczos coefficients via the Lanczos algorithm, but due to a large system size and the instability the algorithm, we do not trust the accuracy of the last coefficients. The larger n Lanczos coefficients will affect larger n probability amplitudes. Due to the factor n weighting in the K-complexity sum, inaccuracies to large n Lanczos coefficients can have amplified impact on the K-Complexity.

The recursive probability amplitude formula (RPF) presented in the following subsection avoids the boundary error encountered in case one, by not requiring fixing the Schrödinger equation boundary. Instead, it utilizes both the return amplitude, and the Lanczos coefficients to recursively generate the probability amplitudes from derivatives of

the return amplitude. When using probability amplitudes generated using this method, the sum of the total probability amplitudes provides an accurate measure of the fraction of total information captured by our truncated set at time t. More specifically, we can use the RPF to estimate the error in the K-complexity derived from the truncated set of Lanczos coefficients, relative to the true K-complexity. This is a critically useful measure in case two, which we encounter for later results in this work. The major limitation of this technique is that it requires both some Lanczos coefficients and an exact closed expression for the return amplitude, which inhibits its usage for many systems.

4.2 The Recursive Probability Formula

Suppose we have both the return amplitude of our reference operator, $\mathcal{O}$, and an incomplete set of Krylov operators of length N, from our incomplete set of Lanczos coefficients. Recall that the n'th probability amplitude is the projection of the time-evolved operator onto the n'th Krylov basis operator. We rewrite the Schrödinger equation for the probability amplitudes in terms of these projections as

$$i\partial_t(K_n|\mathcal{O}(t)) = a_n(K_n|\mathcal{O}(t)) + b_n(K_{n-1}|\mathcal{O}(t)) + b_{n+1}(K_{n+1}|\mathcal{O}(t)). \tag{4.1}$$

Re-arranging the above equation i.t.o. the $(K_{n+1}|\mathcal{O}(t))$ term, we get

$$(K_{n+1}|\mathcal{O}(t)) \;=\; \frac{1}{b_{n+1}}\left[i\partial_t(K_n|\mathcal{O}(t)) - a_n(K_n|\mathcal{O}(t)) - b_n(K_{n-1}|\mathcal{O}(t))\right] . \tag{4.2}$$

We can see that probability amplitudes are exactly determined by the preceding ones. We can thus construct a recursive formula to generate the overlaps for higher n in terms of $(K_0|\mathcal{O}(t))$:

$$\begin{aligned}
(K_1|\mathcal{O}(t)) \;&=\; \frac{1}{b_1}\left[i\partial_t(K_0|\mathcal{O}(t))\right] && (4.3)\\
&\equiv k_1(K_0|\mathcal{O}(t)) && (4.4)\\
(K_2|\mathcal{O}(t)) \;&=\; \frac{1}{b_2}\left[i\partial_t k_1 - a_1k_1 - b_1k_0\right](K_0|\mathcal{O}(t)) && (4.5)\\
&\equiv k_2(K_0|\mathcal{O}(t)) && (4.6)\\
(K_3|\mathcal{O}(t)) \;&=\; \frac{1}{b_3}\left[i\partial_t k_2 - a_2k_2 - b_2k_1\right](K_0|\mathcal{O}(t)) && (4.7)\\
&\equiv k_3(K_0|\mathcal{O}(t)) . && (4.8)
\end{aligned}$$

From this we can identify that [62],

$$\begin{aligned}
(K_{n+1}|\mathcal{O}(t)) \;&=\; \sum_{m=0}^{n+1} k_{m,n+1}\,\partial_t^m(K_0|\mathcal{O}(t)) , && (4.9)\\
k_{m,n+1} \;&=\; \frac{ik_{m-1,n} - a_nk_{m,n} + b_nk_{m,n-1}}{b_{n+1}} ;. && (4.10)
\end{aligned}$$

Equations 4.9 and 4.10 are convenient for recursively generating probability amplitudes, $\phi_n(t)$, if we have full knowledge of the return amplitude $C(t) = \phi_0(t) = (K_0|\mathcal{O}(t))$.

4.3 Error estimates

The probability amplitudes can be used to get an error estimate for the resulting K-Complexity. We will use the fact that all the probability amplitudes should sum to 1, i.e.

$$\sum_{n=0}^{\mathcal{K}_D} |\phi_n(t)|^2 \;=\; 1 \;, \tag{4.11}$$

where $\mathcal{K}_D$ the dimension of the Krylov space. Suppose we have a truncated set of Lanczos coefficients of length N, and thus have the first N probability amplitudes. As the operator grows, it spreads along the Krylov chain, requiring additional Krylov basis operators to describe it. However, due to the truncation, our description of the dynamics will become inaccurate after some time. This will be the point at which a precise description of the time-evolved operator necessitates Krylov basis vectors not within our truncated set. A useful measure of the amount of the operator captured by the known probability amplitudes would simply be sum of the known probability amplitudes. A simple error measure would then be

$$\varepsilon_0(t) \;=\; 1 - \sum_{n=0}^{N} |\phi_n(t)|^2 \;. \tag{4.12}$$

This error measure will be 0 for all t where the operator's dynamics are fully captured by the set of known probability amplitudes i.e. $\{\phi_n : n \leq N\}$.

When $\varepsilon_0(t) > 0$, the missing support of the operator lies somewhere in the set $\{\phi_n : N < n \leq \mathcal{K}_D\}$. Recall that our definition of K-Complexity is the average position of the operator's support along the Krylov Chain, $K(t) = \sum_n n|\phi_n(t)|^2$. Here we can see that the ϕ_n's are weighted more for larger n. If the missing support is captured by the very next probability amplitude, ϕ_{N+1}, (i.e. the only other Krylov basis vector necessary to describe $\mathcal{O}(t)$ is K_{N+1}) then the error in the K-Complexity will be simply $(N+1) \times \varepsilon_0(t)$. This provides a minimum bound for the truncation error of the K-Complexity,

$$\varepsilon_1(t)_{\text{min}} \;=\; (N+1)\, \varepsilon_0(t) \;. \tag{4.13}$$

Similarly, the worst case scenario would be that the missing support is the very last Krylov vector—the one with the largest weight—offering the maximum bound for the K-Complexity truncation error,

$$\varepsilon_1(t)_{\text{max}} \;=\; (\mathcal{K}_D - 1)\, \varepsilon_0(t) \;. \tag{4.14}$$

A clear drawback of this error estimate is that the Krylov dimension is a necessary parameter. For our use in this work, the fairly consistent sawtooth shape of the Lanczos coefficients allows for extrapolation and a decent estimate. However, we can simply make an extremely conservative upper bound by using the Hilbert space size.

It is very natural to now ask: can we improve this upper bound on the error? The answer is nuanced. This bound, 4.14, can in fact be saturated in the canonical example of the $SU(2)$ Liouvillian $L = \alpha(J_+ + J_-)$, with the reference operator being the lowest weight state $|j, -j\rangle$. The Krylov basis is given by $|K_n) = |j, j+n\rangle$ for $n = 0, 1, \ldots, 2j$. This gives us a Krylov dimension of $K_D = 2j + 1$ equal to the Hilbert space size. The

resulting probability amplitudes are $\phi_n(t) = \frac{\tan^n(\alpha t)}{\cos^{-2j}(\alpha t)}\sqrt{\frac{\Gamma(2j+1)}{n!\Gamma(2j-n+1)}}$ [33]. The evolution of the probability amplitudes is such that it is possible to have all the probability concentrated in the highest and lowest weight states at various times. For instance, at $t = \frac{\pi}{2\alpha}$ the magnitude of the final probability amplitude is $|\phi_{K_D-1}(\frac{\pi}{2\alpha})|^2 = 1$. This means that for any truncated set of Krylov operators where we have $\{|K_n)\}_{n=0}^{N}$ for $N < K_D - 1$, there exists a time, t, where all the support lies on $\{|K_n)\}_{n=N+1}^{K_D-1}$. Thus, the error bound given in Equation 4.14 will be saturated. Note that this does not in any way rule out meaningful improvements to the error bound. This simply rules out bounds of the form $C\,\epsilon_0(t)$, for some constant $C < K_D - 1$.

It is possible that bounds on the K-complexity error can be approached from the perspective of quantum speed limits. Lieb-Robinson type bounds [63] have been formulated for the Krylov complexity operator, resulting in universal speed limits to the growth of K-complexity [64], with recent extensions to open systems [65].

This top-down speed limits approach incorporates dynamical constraints on the Lanczos coefficients which our error analysis above does not incorporate. However, we believe that a naive speed-limits approach is likely to overestimate the error for most systems, making analyses of the distribution of probability amplitude, such as the error analysis above, more robust.

5 Spin chain background

In this section we begin with a brief overview of spin chains and the canonical commutation relations for fermions, followed by an introduction of the Jordan-Wigner transformation as a general map between spin systems and spinless fermions. Next, we present the specific models central to this work: the Transverse Field Ising model, and the Kitaev chain. Finally, we present a thorough account of how these two systems are related via the Jordan-Wigner transformation.

5.1 Spin operators and commutation relations

A single spin-1/2 particle has a complex two-dimensional Hilbert space $\mathcal{H}_i$. The spin observables of our spin-1/2 system are the three spin operators $\hat{S}^x, \hat{S}^y, \hat{S}^z$, which can be represented by the Pauli matrices through the relation $\hat{S}^\alpha = \frac{\hbar}{2}\sigma^\alpha$, where $\alpha = \{x, y, z\}$ [66]. For simplicity, we will omit the $\frac{\hbar}{2}$ factor and use the Pauli matrices directly as our spin operators. A quantum state in this Hilbert space can be described by a two-component complex vector called a spinor. As a basis, we often use the eigenstates of the σ^z matrix, denoted $|\uparrow\rangle$ and $|\downarrow\rangle$, corresponding to the eigenvalues $+1$ and -1 respectively.

For a spin chain, the Hilbert space is constructed as the tensor product of the representations of the single particle spin-1/2 Hilbert spaces, $\mathcal{H} = \bigotimes_j \mathcal{H}_j$. We can define spin operators σ_j^α that act on the two-dimensional subspace associated with each site j, where $\alpha = \{x, y, z\}$. These spin operators, acting only on their own respective subspace, will commute at different sites,

$$[\sigma_i^\alpha, \sigma_j^\beta] = 0, \quad \text{where} \quad i \neq j \ . \tag{5.1}$$

When acting on the same site, σ_j^α has the usual commutation rule for Pauli matrices,

$$[\sigma_j^\alpha, \sigma_j^\beta] = 2i\varepsilon^{\alpha\beta\gamma}\sigma_j^\gamma \ , \tag{5.2}$$

where $\varepsilon^{\alpha\beta\gamma}$ is the Levi-Civita symbol. The matrices $i\sigma^x, i\sigma^y, i\sigma^z$ form a basis for the Lie algebra $\mathfrak{so}(3) \cong \mathfrak{su}(2)$, which is the associated Lie algebra of the 3D rotation group $SO(3)$ [67].

We can define raising and lowering spin operators as

$$\sigma_i^\pm \ = \ \frac{1}{2}\left(\sigma_i^x \pm i\sigma_i^y\right) \ , \tag{5.3}$$

which act on the σ^z eigenstate basis as $\sigma^+|\downarrow\rangle = |\uparrow\rangle$ and $\sigma^-|\uparrow\rangle = |\downarrow\rangle$. The spin raising and lowering operators also satisfy the anti-commutation relations

$$\{\sigma_i^-, \sigma_i^+\} \ = \ 1 \ , \qquad\qquad \{\sigma_i^+, \sigma_j^+\} = \{\sigma_i^-, \sigma_j^-\} = 0 \ , \tag{5.4}$$

or in terms of commutation relations,

$$[\sigma_i^+, \sigma_j^-] = \delta_{ij}\sigma_j^z \ , \qquad\qquad [\sigma_i^+, \sigma_j^+] = [\sigma_i^-, \sigma_j^-] = 0 \ . \tag{5.5}$$

Putting the spin operators to the side for the moment, we can discuss canonical commutation relations (CCR). Given a set of operators $c_1, \ldots, c_L$ which act on some Hilbert space $\mathcal{H}_F$, we say that these operators satisfy *canonical commutation relations (CCRs) for fermions* [68] if

$$\{c_i, c_j^\dagger\} = \delta_{ij} I \,, \qquad \{c_i, c_j\} \;=\; \{c_i^\dagger, c_j^\dagger\} \;=\; 0 \,. \tag{5.6}$$

In the context of a fermionic system, operators $c_j^\dagger$ and c_j which satisfy CCR are referred to as creation and annihilation operators, respectively. The application of a creation (annihilation) operator to a fermionic state adds (removes) a particle from the state. The fermionic state could be many-body wavefunction in first quantization, or a Fock space state in second quantization. A Fock space state is a linear combination of n-particle states, with contributions for each n, and can be constructed by the action of some combination of creation and annihilation operators on the vacuum.

The canonical commutation relations (CCRs) can be viewed as a set of mathematical conditions that define a family of operators. If we take this perspective, the important question becomes: what are the consequences of operators satisfying CCRs? In Appendix D, we explore the mathematical implications of this on the structure of the fermionic Hilbert space, $\mathcal{H}_F$. The key result is that the algebra defined by imposing fermionic CCRs on the operators $c_1, \ldots, c_L$ enables a simple and elegant representation of fermionic modes that respect Fermi statistics. In particular, as we demonstrate in D, imposing CCRs gives $\mathcal{H}_F$ a structure that naturally leads to the occupation number representation for fermions, corresponding to the fermionic Fock space.

5.2 The Jordan-Wigner transformation

The Jordan-Wigner (JW) transformation allows fermionic variables to be re-expressed in terms of spin variables. Specifically, it expresses fermionic creation and annihilation operators as combinations of Pauli matrices while preserving the correct fermionic canonical anticommutation relations [68, 69]. The Jordan-Wigner transformation is an incredibly useful tool—it can allow us to leverage the extensive literature on many-body methods for bosonic and fermionic systems [70] to learn about spin systems. For example, we can map interesting spin systems like the quantum XY model to quadratic fermionic systems that can be solved straightforwardly [68, 71], see Appendix C.1.

This approach exemplifies the broader utility of duality transformations—by mapping a system onto a mathematically equivalent one, with the same physical degrees of freedom, we may be able to gain new insights into the original system. Such transformations are often described as introducing a *quasiparticle description* of the original system. This is foundational in modern physics and has been crucial to understanding processes such as superconductivity and the quantum Hall effect [68].

In this subsection we will first establish the mapping between spin operators and hard-core bosons, and then introduce the *Jordan-Wigner string*—an additional factor that will modify the inter-site commutation relations to match that of a fermionic system.

With a single boson $b^\dagger$ we can construct an infinite dimensional Hilbert space by acting on the associated vacuum state $|0\rangle$ repeatedly. Thus it seems impossible to describe spins

using bosons. However, we can truncate the Hilbert space to only two states $\{|0\rangle, |1\rangle\}$ where $b^\dagger|0\rangle = |1\rangle$ by simply enforcing that $(b^\dagger)^2|0\rangle = 0$. This is known as a *hard-core boson*, and can be described by the addition of an infinite on-site repulsion term to the boson Hamiltonian [71]. This hard-core constraint takes the form of changing the same-site commutation rule to anticommute instead; with $\{b_j^\dagger, b_j^\dagger\} = \{b_j, b_j\} = 0$, and $\{b_j, b_j^\dagger\} = 1$. We can see that this enforces single occupancy at each site—equivalent to the Pauli exclusion principle.

To map the spin matrices to the hard-core bosons, we first identify the states at each site as $|0\rangle \leftrightarrow |\uparrow\rangle$ and $|1\rangle \leftrightarrow |\downarrow\rangle$.

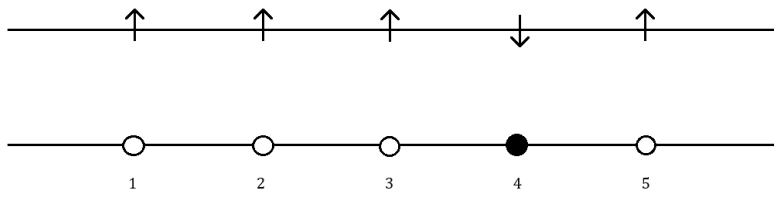

Figure 1. Diagram of a 1D 5-site spin chain configuration, with a corresponding particle-hole configuration given by $b_4^\dagger|0\rangle$.

In order to have the correct action on the states, i.e. $\sigma^+|\downarrow\rangle = |\uparrow\rangle$ and $\sigma^-|\uparrow\rangle = |\downarrow\rangle$, we get the following mapping:

$$\sigma_j^+ = b_j \ , \tag{5.7}$$

$$\sigma_j^- = b_j^\dagger \ , \tag{5.8}$$

$$\sigma_j^z = 1 - 2b_j^\dagger b_j \ . \tag{5.9}$$

Using $\sigma_i^\pm = (\sigma_i^x \pm i\sigma_i^y)/2$ we can also obtain

$$\sigma_j^x = b_j^\dagger + b_j \ , \tag{5.10}$$

$$\sigma_j^y = i(b_j^\dagger - b_j) \ . \tag{5.11}$$

Let us now consider the mapping of the spin and hard-core operators to fermionic operators. Fermionic operators anticommute at different sites, whereas the spin and hard-core boson operators do not. Commuting of neighbouring fermionic variables thus picks up a minus sign, and commuting an operator past multiple neighbours requires keeping track of the number of operators passed. Due to this property of the fermions, the Jordan-Wigner mapping is only possible in one dimension, where the sites can be naturally ordered [71].

To map the inter-site bosonic commutation relation to the fermionic counterpart, we need an operator that can "count" the number of sites between the operators and assign the appropriate -1 or $+1$ factor. The necessary operator is called the *Jordan-Wigner string* and is given by

$$S_j \ = \ \exp\left(i\pi \sum_{l=1}^{j-1} c_l^\dagger c_l\right) \ = \ \prod_{l=1}^{j-1} \left(1 - 2c_l^\dagger c_l\right) \ , \tag{5.12}$$

where we can see that this operator produces a phase equal to $+1$ or -1 depending on the parity of the number of fermions before site j. Note that this is a highly non-local operator, with $S_j = S_j^\dagger = S_j^{-1}$, and thus has eigenvalues ± 1.

Using this we can write our spin and hard-core boson operators in terms of the fermionic operators, thus defining our *Inverse Jordan-Wigner transformation* (IJW):

$$\sigma_j^+ \;=\; b_j \;=\; S_j c_j \;=\; \prod_{l=1}^{j-1}\left(1-2c_l^\dagger c_l\right) c_j \;, \tag{5.13}$$

$$\sigma_j^- \;=\; b_j^\dagger \;=\; S_j c_j^\dagger \;=\; \prod_{l=1}^{j-1}\left(1-2c_l^\dagger c_l\right) c_j^\dagger \;, \tag{5.14}$$

$$\sigma_j^z \;=\; 1-2b_j^\dagger b_j \;=\; 1-2c_j^\dagger c_j \;. \tag{5.15}$$

This transformation can be inverted using the σ^z equation to arrive at the *Jordan-Wigner transformation* (JW):

$$c_j = \prod_{l<j}(\sigma_l^z)\,\sigma_j^+ \;, \tag{5.16}$$

$$c_j^\dagger = \prod_{l<j}(\sigma_l^z)\,\sigma_j^- \;, \tag{5.17}$$

where the product above denotes a Kronecker tensor product.

For a 1D chain of length L we can write down the following form for its creation and annihilation operators in terms of Pauli spin operators, making the products explicit:

$$c_j \;=\; \Big(\bigotimes_{l<j}\sigma_l^z\Big)\otimes\sigma_j^+\otimes\Big(\bigotimes_{j<l<L} I_l\Big) \;, \tag{5.18}$$

$$c_j^\dagger \;=\; \Big(\bigotimes_{l<j}\sigma_l^z\Big)\otimes\sigma_j^-\otimes\Big(\bigotimes_{j<l<L} I_l\Big) \;. \tag{5.19}$$

5.3 Transverse field Ising Model

The quantum Ising chain provides a brilliant environment for studying fundamental quantum dynamics, phase transitions and non-equilibrium dynamics [71, 72]. In general the transverse field Ising model features a nearest-neighbour interaction determined by the alignment or anti-alignment of spin projections along a given axis (e.g., the z-axis), while a transverse field introduces a directional bias for spin projections perpendicular to the interaction (e.g, along the x-axis).

Each spin in the quantum Ising chain is a qubit, i.e. it can be described by states that are quantum superpositions of two basis states, the spin up state and the spin down state. As such, a spin in the quantum Ising chain can be in any one of an infinite set of states. This contrasts with the classical Ising model, where the spin degree of freedom can only have two states, $\sigma = 1$ or $\sigma = -1$. Notably, for these qubits, the spin projections along the

x and z axes do not commute. This corresponds to the fact that these observables cannot be measured simultaneously, a consequence of the uncertainty principle.[8]

We will restrict our discussion to the one-dimensional (1D) lattice, with each lattice site being a 2D complex Hilbert space representing spin-1/2 particle. The 1D transverse field quantum Ising Model (TFIM) Hamiltonian is given by

$$H_{\text{Ising}} \;=\; -J\sum_{\langle ij\rangle}\sigma_i^x\sigma_j^x - Jg\sum_i \sigma_i^z \;, \tag{5.20}$$

where $\sigma_i^{x,y,z}$ are the Pauli matrices at site i, $\langle ij\rangle$ denotes a set of neighbouring sites, and g is the magnetic field strength or coupling parameter. We will assume a ferromagnetic interaction between neighbouring spins, i.e. $J > 0$, and we assume $g \geq 0$ without loss of generality. It is important to note that the TFIM system contains a $\mathbb{Z}_2$ symmetry—it is invariant under the flipping of all the spins in the x-direction—an action given by the unitary transformation $\hat{\xi} = \prod_i \sigma_i^z$.

The TFIM exhibits a quantum phase transition (QPT) between two phases: the so-called *ordered phase* whose ground state breaks the $\hat{\xi}$ spin-flip symmetry ($\langle\sigma^x\rangle \neq 0$), and the *disordered phase*, whose ground state preserves the $\hat{\xi}$ symmetry ($\langle\sigma^x\rangle = 0$) [72].

For $g < 1$, the system is in the *ordered phase*. In this phase the system has two degenerate ground states where the spins are aligned with positive or negative x-direction. However, for a finite size chain, there is a finite probability for tunneling between the two ground states which is suppressed exponentially in the system size. This can be interpreted as a quantum ferromagnet ($g \to 0$) with its ground state degeneracy lifted by adding an L'th order perturbation of a transverse field, $V = -Jg\sum_i \sigma_i^z$, where L is the number of sites, resulting in exponentially small splitting between the lowest energy states. This ordered phase is also *gapped*—meaning that the lowest energy excited states are separated from the ground state by a non-zero energy gap that does not vanish in the thermodynamic limit. The energy gap in the ordered phase is $2J(1-g)$ [73].

For $g > 1$, the system is in its *disordered phase*, or paramagnetic phase. This regime is also part of the gapped phase, with an energy gap of $2J(g-1)$ [73].

At $g = 1$ the system undergoes the quantum phase transition between the ordered and disordered phases. This critical point is also the gapless phase. At the critical point the system displays a number of interesting symmetries. The TFIM can be mapped, using imaginary-time slicing, to the 2D classical Ising model [73], which at criticality can be reduced to the 2D Ising CFT in the low energy limit. This is a 2D CFT with a central charge of $c = \frac{1}{2}$ [74]. We can, in fact, also recover the 2D Ising CFT from the TFIM via a Jordan-Wigner transformation, and diagonalizing the resulting Kitaev chain, as seen in Appendix C.

[8] In 1922, the Stern-Gerlach experiment with the sequential z-axis, x-axis, z-axis measurement setup showed that angular momentum cannot be measured on two perpendicular axes at the same time. Suppose at the first measurement we filter for particles with their z projection measured to be $z+$. The subsequent measurement of the spin projection in the x direction 'destroys' the information on the previous z direction measurement. The final measurement of the z projection thus measures both $z+$ and $z-$.

The TFIM is a limit of the quantum XY Model, which considers an interaction in both directions perpendicular to the magnetic field (here x and y). The XY Model is itself a limit of the general quantum Heisenberg model which considers x, y, and z interactions,

$$H_{\text{Heisenberg}} = -\sum_{j=1}\left(J_x\sigma_j^x\sigma_{j+1}^x + J_y\sigma_j^y\sigma_{j+1}^y + J_z\sigma_j^z\sigma_{j+1}^z + h\sigma_j^z\right) . \tag{5.21}$$

Two well studied cases are $J_x = J_y \neq J_z$, known as the XXZ model, and the case where $J_x = J_y = J_z$, known as the XXX model. The Bethe Ansatz can be used to exactly solve the one-dimensional Heisenberg XXX and XXZ models for arbitrary spin [75–77]. These more general models will not be directly studied in this work, however, as we will see, the XY model may provide a useful extension to our scope.

5.3.1 Kramers-Wannier Duality

The ordered and disordered phases of the TFIM can be mapped to each other through a non-local Kramers-Wannier type duality. Consider the mapping from spins to domain wall variables,

$$s_{\bar{i}}^z = \sigma_i^x\sigma_{i+1}^x , \qquad s_{\bar{i}}^x s_{\bar{i}}^x = \prod_{i>\bar{i}}\sigma_i^z , \qquad \text{where } \bar{i} = i + \frac{1}{2} . \tag{5.22}$$

Through this we can arrive at the dual Hamiltonian,

$$H_{\text{KW}} = -J\sum_{\bar{i}} s_{\bar{i}}^z - Jg\sum_{\langle\bar{i}\bar{j}\rangle} s_{\bar{i}}^x s_{\bar{j}}^x , \tag{5.23}$$

which we can recognize as equivalent to H_{Ising} with the coupling exchange $J \leftrightarrow gJ$. Here we can see that the ordered and disordered phases map to one another for $g \neq 1$ while we have a self-dual point at $g = 1$.

5.4 The Kitaev Chain

The Kitaev chain is a one-dimensional model describing a tight-binding chain of spinless fermions. The Kitaev chain Hamiltonian with general twisted boundary conditions is given by

$$\begin{aligned} H_{\text{Kitaev}} = \sum_{j=1}^{L-1}\left[-\frac{t}{2}\left(c_{j+1}^\dagger c_j + c_j^\dagger c_{j+1}\right) + \frac{\Delta}{2}\left(c_j^\dagger c_{j+1}^\dagger + c_{j+1}c_j\right)\right] - \sum_{j=1}^{L}\mu\, c_j^\dagger c_j \\ + a\left[-\frac{t}{2}\left(c_1^\dagger c_L + c_L^\dagger c_1\right) + \frac{\Delta}{2}\left(c_L^\dagger c_1^\dagger + c_1 c_L\right)\right] , \end{aligned} \tag{5.24}$$

where c_j and $c_j^\dagger$ are annihilation and creation operators for spinless fermions acting on site j. The real parameters t and μ are known as the hopping amplitude and chemical potential respectively, and Δ is the superconducting strength which is generally a complex parameter. The boundary factor $a = \{-1, 0, 1\}$ encodes the possible boundary conditions of anti-periodic, open, and periodic boundary conditions respectively.

The Kitaev chain also exhibits a topological phase transition at $|\frac{\mu}{t}| = 1$. For $|\frac{\mu}{t}| < 1$ the system is topologically non-trivial, and exhibits Majorana Zero Modes (MZMs) [41, 78, 79]. MZMs are of key importance in the field of quantum computing. In particular, they are useful in the construction of qubits immune to decoherence by both bit-flip errors and dephasing [79]. For further discussion on these properties of the Kitaev chain, see Appendix C.3.

It is important to note that the number of fermions, $\hat{N}$, is *not* conserved by the Hamiltonian, due to the superconducting terms. However, the parity of the number of fermions $(-1)^{\hat{N}}$ is conserved. We can express the fermion parity as

$$\hat{\mathcal{P}} \;=\; \prod_{j=1}^{L}(1-2c_j^\dagger c_j) \;=\; e^{i\pi\sum_{l=1}^{L}c_l^\dagger c_l}\;, \tag{5.25}$$

where $\hat{\mathcal{P}}$ returns the eigenvalues $+1$ or -1 for states with even and odd parity respectively.

In Appendix C we solve explicitly for the spectrum of the Kitaev chain, and discuss its behaviour at criticality. We also discuss more of the properties of the Kitaev chain via discussion on the fermionic representation of the TFIM in sections 5.5 and 5.6.

5.5 Ising Chain to Kitaev Chain

1D Transverse-field Quantum Ising Model (TFIM) can be mapped via the Inverse Jordan-Wigner transformation to a system of spinless fermions, namely the Kitaev Chain. The Inverse Jordan-Wigner transform can be performed by making the substitution,

$$\sigma_i^z \;\to\; 1-2c_i^\dagger c_i\;, \tag{5.26}$$

$$\sigma_i^x \;\to\; \prod_{j<i}(1-2c_j^\dagger c_j)(c_i^\dagger + c_i)\;. \tag{5.27}$$

Some algebraic manipulation yields a substitution for the interaction term,

$$\sigma_i^x\cdot\sigma_{i+1}^x \;\to\; c_i^\dagger c_{i+1}^\dagger + c_i^\dagger c_{i+1} - c_i c_{i+1}^\dagger - c_i c_{i+1}\;. \tag{5.28}$$

Making the simple substitution of 5.26 and 5.28 into H_{Ising} yields:

$$H_{\text{JW}} = -\sum_j \left[J\left(c_{j+1}^\dagger c_j + c_j^\dagger c_{j+1}\right) \;-\; 2Jg\, c_j^\dagger c_j + g \;+\; J\left(c_j^\dagger c_{j+1}^\dagger + c_{j+1}c_j\right)\right]. \tag{5.29}$$

We can identify this as the Kitaev Chain Hamiltonian with the tight-binding coefficient and the superconducting term coefficient having equal strength J, and the chemical potential term with strength $2Jg$. The IJW mapping from H_{Ising} to H_{JW} presented above is the critical transformation for this work. It should be noted however that this mapping is more general—in fact the Kitaev Chain can be mapped to the 1D quantum XY Model without constraints on the Kitaev chain parameters [80]. Directly substituting the Jordan-Wigner transformation 5.16 and 5.17 into H_{Kitaev}, we arrive at

$$H_{\text{XY}} \;=\; \sum_j -\frac{t}{2}\left(\sigma_{j+1}^+\sigma_j^- + \sigma_{j+1}^-\sigma_j^+\right) - \frac{\mu}{2}(\sigma_j^z - 1) + \frac{\Delta}{2}\left(\sigma_{j+1}^+\sigma_j^+ + \sigma_{j+1}^-\sigma_j^-\right) \tag{5.30}$$

$$\;=\; \frac{\mu N}{2} - \left(\sum_j \frac{t+\Delta}{4}\sigma_{j+1}^x\sigma_j^x + \frac{t-\Delta}{4}\sigma_{j+1}^y\sigma_j^y + \frac{\mu}{2}\sigma_j^z\right). \tag{5.31}$$

The TFIM with periodic boundary conditions (PBCs) does not map trivially to the periodic Kitaev chain. To investigate the difference, consider the boundary term added to the open Ising chain to arrive at the periodic Ising chain, $\sigma_L^z\sigma_1^z$. This boundary term transforms under the Inverse Jordan-Wigner transformation as,

$$\sigma_L^x\sigma_1^x \rightarrow \prod_{j=1}^{L-1}(1-2c_j^\dagger c_j)(c_L^\dagger + c_L)(c_1^\dagger + c_1)\ , \tag{5.32}$$

$$= \prod_{j=1}^{L}(1-2c_j^\dagger c_j)(c_L - c_L^\dagger)(c_1^\dagger + c_1)\ , \tag{5.33}$$

$$= S_{L+1}(c_L - c_L^\dagger)(c_1^\dagger + c_1)\ . \tag{5.34}$$

This is a highly non-local operator, quite different to the operators to which bulk terms of the Ising Hamiltonian map. For comparison the boundary term of Kitaev Chain with PBC's is

$$(c_L^\dagger - c_L)(c_1 + c_1^\dagger) \ = \ c_L^\dagger c_1^\dagger + c_L^\dagger c_1 - c_L c_1^\dagger - c_L c_1\ . \tag{5.35}$$

There is a clear difference between the PBC Kitaev chain boundary term and the PBC Ising boundary term after mapping under the Inverse Jordan-Wigner transformation. However, note that these two boundary terms are directly related by the multiplication of a Jordan-Wigner string S_{L+1}, since $S_j = S_j^{-1}$. To avoid confusion we will refer to the periodic Kitaev chain as H_{Kitaev}, and use H_{JW} for the fermionic Hamiltonian resulting from the Inverse Jordan-Wigner map on the periodic TFIM, i.e.

$$H_{\text{Kitaev}} \ = \ H_{\text{OBC Kitaev}} + (c_L^\dagger - c_L)(c_1^\dagger + c_1) \tag{5.36}$$

$$H_{\text{JW}} \ = \ H_{\text{OBC Kitaev}} - S_{L+1}(c_L^\dagger - c_L)(c_1^\dagger + c_1)\ . \tag{5.37}$$

We will refer to the boundary term of H_{JW} as the Jordan Wigner twist. This twist has nontrivial consequences for the symmetries in operator and spread complexities of fermionic operators. We shall tug on this string further in Section 8.1.

We can see that H_{JW} will have the fermion parity symmetry of Kitaev chain. It will be convenient to define projection operators for the even and odd subspaces,

$$\hat{\mathcal{P}}^+ = \frac{1}{2}(I + e^{i\pi\hat{N}})\ , \qquad \hat{\mathcal{P}}^- = \frac{1}{2}(I - e^{i\pi\hat{N}})\ . \tag{5.38}$$

Since the Hamiltonian does not mix parity sectors, we may conveniently split it and write it in block diagonal form,

$$H_{\text{JW}} \ = \ H_{\text{JW}}^+ + H_{\text{JW}}^- \ = \ \begin{pmatrix} H_{\text{JW}}^+ & 0 \\ 0 & H_{\text{JW}}^- \end{pmatrix}\ , \tag{5.39}$$

where $H_{\text{JW}}^+ = \hat{\mathcal{P}}^+ H_{\text{JW}} \hat{\mathcal{P}}^+$ and $H_{\text{JW}}^- = \hat{\mathcal{P}}^- H_{\text{JW}} \hat{\mathcal{P}}^-$ are the projections of H_{JW} onto the even and odd parity sectors respectively.

In the parity odd sector we have that $S_{L+1} = -1$, thus from Equation 5.37, it is clear that H_{JW}^{-} is a periodic fermionic Hamiltonian. It is in fact exactly the Kitaev chain with periodic boundary conditions (PBCs). Similarly, in the parity even sector of H_{JW} where $S_{L+1} = 1$, H_{JW}^{+}, is exactly the Kitaev chain with anti-periodic boundary conditions (APBCs).

5.6 Corresponding symmetry phases

The classification of the phases for 1D spin systems and their corresponding fermionic formulations has been well studied [81–83]. Recall that in the ferromagnetic phase, $g < 1$, the TFIM has a two-fold ground state degeneracy, where at finite size it has splitting that is exponentially small in the system size. The ground state of the TFIM breaks the $\hat{\xi} = \prod_{j=1}^{L} \sigma_j^z$ symmetry of the system. The Jordan-Wigner transformation maps this symmetry operator to the parity operator of the fermionic formulation,

$$\hat{\xi} = \prod_{j=1}^{L} \sigma_j^z \;\leftrightarrow\; \hat{\mathcal{P}} = \prod_{j=1}^{L} (1 - 2c_j^\dagger c_j) \; . \tag{5.40}$$

The two eigenstates of the parity operator can be written in terms of the ferromagnetic spin ground states,

$$|\psi_\pm\rangle = \frac{1}{\sqrt{2}} \Big(|+, + \ldots, +\rangle \pm |-, -, \ldots, -\rangle \Big) \; , \tag{5.41}$$

where $|+\rangle$ and $|-\rangle$ are the eigenstates of σ^x with eigenvalues ± 1. These states, $|\psi_\pm\rangle$, can be represented by the two fermionic ground states of the parity-even and parity-odd sectors [71].

The spectrum of the fermionic Hamiltonian H_{JW} can be computed via a discrete Fourier transform, followed by a reformulation in terms of quasi-particle superpositions of particles and holes known as Bogoliubons. We compute this explicitly in Appendix C. The ground state of this fermionic system is the Bogoliubov vacuum—we can define one such vacuum for each of the odd and even sectors. The double degeneracy of the TFIM ground states corresponds then to the two fermionic ground states of each parity sector. The symmetric phase of the TFIM, or paramagnetic phase, maps trivially. We then have than both the spin symmetry breaking, and the spin symmetric phases correspond to symmetric fermion phases [81].

6 Numerical methods

For numerical implementation, we can use matrix representations for all the operators and states in the TFIM system. The Pauli matrices,

$$\bar{\sigma}_x = \begin{pmatrix} 0 & 1 \\ 1 & 0 \end{pmatrix} , \qquad \bar{\sigma}_y = \begin{pmatrix} 0 & -i \\ i & 0 \end{pmatrix} , \qquad \bar{\sigma}_z = \begin{pmatrix} 1 & 0 \\ 0 & -1 \end{pmatrix} , \tag{6.1}$$

are a faithful representation[9] of our spin-1/2 operators, $\{\sigma^x, \sigma^y, \sigma^z\}$. Recall that the full Hilbert space of the TFIM is constructed from a tensor product of single-site Hilbert spaces. Each single-site Hilbert space is a real vector space of 2×2 Hermitian matrices, spanned by the set $\{\bar{\sigma}_x, \bar{\sigma}_y, \bar{\sigma}_z, \mathbb{I}_2\}$, and thus the operator space for the TFIM chain of length L has a total dimension of 4^L. For a chain of length L, we can construct operators for the full system from a Kronecker tensor product of the matrix representations of the operators for each respective site.

6.1 Lanczos Algorithms

The *Lanczos algorithm* was developed by C. Lanczos as an iterative method to solve the eigenvalue problem for linear differential and integral operators [4]. The Lanczos algorithm primarily functions as a tridiagonalization procedure, approximating the eigenvalues and eigenvectors of a Hermitian matrix. It does so by constructing an orthogonal basis for the Krylov subspace—the Krylov basis—where the input matrix takes a tridiagonal form [4, 6]. The more general form of the algorithm, applicable to non-Hermitian matrices, is known as the *Arnoldi algorithm* [7].

The primary advantage of the Lanczos algorithm is its ability to yield useful approximations after only a few iterations. However, its major drawback is numerical instability, which can affect the accuracy of the results [9]. For complete tridiagonalization, Householder transformations are generally preferred over the Lanczos algorithm due to their superior numerical stability [9].

For exact arithmetic, the Lanczos algorithm constructs an orthonormal basis [84]. However, when implemented with finite-precision arithmetic, numerical errors cause the algorithm to generate non-orthognal elements [8, 9]. Remedies to the instability include full re-orthogonalization (using the stable modified Gram-Schmidt procedure), partial re-orthogonalization procedures, and restarted variations [84, 85].

It is important to track the floating point precision loss at each iteration and make sure the remaining precision does not fall below the desired tolerance. Each float multiplication loses around $\log_{10}(2) \approx 0.3$ decimals of precision. Thus, for N iterations and N Lanczos coefficients we need more than $N/3$ digits of precision. For large systems this requires the usage of arbitrary precision floats. Arbitrary precision floats are extremely inefficient in languages such as Julia (using BigFloat), but are quite natural in Mathematica. This is the

[9] A representation f of a group G on a vector space V is said to be a *faithful representation* if it is a linear representation in which each element $g \in G$ maps to a unique point $f(g)$, i.e. the group homomorphism $f : G \to GL(V)$ is injective.

primary reason for our use of Mathematica for the implementation of the Lanczos algorithm in this work.

Also note that the Lanczos algorithm terminates when the condition of $b_n = 0$ is met, but when working with finite precision arithmetic, it is necessary to define a convergence tolerance $b_n < b_{\text{tol}}$. If precision drops such that the order of the numerical uncertainty is larger than the tolerance, convergence is no longer guaranteed. In order to guarantee convergence we need to increase the numerical precision by a constant buffer of the number of digits necessary to specify the convergence tolerance, $\sim \log_{10}(b_{\text{tol}}^{-1})$.

Parallelization speed-up is possible for some implementations. The Lanczos algorithm has $O(n)$ points of synchronization, with parallelization points at the level of matrix multiplication.

6.1.1 Basic Lanczos algorithm

The basic normalized Lanczos algorithm for Hermitian operators, follows a Gram-Schmidt procedure. Here we can choose any inner operator product, and our norm is the usual $||O|| = \sqrt{(O|O)}$. The algorithm is as follows:

1. $K_{-1} \equiv 0$
2. $b_0 \equiv 0$, $K_0 \equiv \mathcal{O}/||\mathcal{O}||$
3. For $n \geq 1 : Q_n = \mathcal{L}K_{n-1} - b_{n-1}K_{n-2}$
4. $b_n = ||Q_n||$
5. If $b_n = 0$, stop
6. $K_n = Q_n/b_n$
7. $n = n + 1$, and go to step 3

In this work, we use a Frobenius inner product, which can be replaced by performing a complex dot product with the vectorized version of our matrices. This often allows a significant speed-up. When using finite-precision, numerical instability here *will* cause a loss of orthogonality of the Q_n's.

6.1.2 Arnoldi algorithm

The following generalizes the Lanczos algorithm to include non-hermitian input operators and is known as the *Arnoldi algorithm*. Here the key difference being an additional removal of the 'diagonal' term during the subtraction step. This additional subtraction parameter gives us the a_n Lanczos coefficients. The Arnoldi algorithm is:

1. $K_{-1} \equiv 0$
2. $b_0 \equiv 0$, $K_0 \equiv \mathcal{O}/||\mathcal{O}||$
3. $a_0 = (K_0|\mathcal{L}|K_0)$
4. For $n \geq 1 : Q_n = \mathcal{L}K_{n-1} - a_{n-1}K_{n-1} - b_{n-1}K_{n-2}$
5. $b_n = ||Q_n||$

6. If $b_n = 0$, stop
7. $K_n = Q_n/b_n$
8. $a_n = (K_n|\mathcal{L}|K_n)$
9. $n = n + 1$, and go to step 4

Below the procedure is outlined with alterations to reduce the numerical precision loss in generating the Lanczos coefficients—at the cost of producing unnormalized Krylov basis vectors along the way. The unnormalized Arnoldi algorithm is:

1. $O_1 \equiv \mathcal{O}$; $K_1 = O_1$
2. $A = (O_1|\,\mathcal{L}\,O_1)/||O_1||$; $a_1 = A$
3. $O_2 = \mathcal{L}\,O_1 - A\,O_1$
4. For $n \geq 2$:
   (a) Pre-compute $\mathcal{L}O_2$ and $||O_2||$.
   (b) Compute projections onto previous *and current* basis vectors:
   $A = (O_2|\,\mathcal{L}\,O_2)/||O_2||$
   $B = (O_1\,|\mathcal{L}\,O_2)$
   (c) Orthogonalize by subtracting off the projections:
   $O_3 = \mathcal{L}\,O_2 - A\,O_2 - \frac{B}{||O_1||}\,O_1$
   (d) If $\frac{B}{||O_1||} = 0$, stop.
   (e) Extract the Lanczos coefficients and unnormalized Krylov vectors:
   $a_n = A$;
   $b_n = B/\sqrt{||O_1||\,||O_2||}$;
   $K_n = O_1$
   (f) Reassign the following and go to step 4:
   $O_1 = O_2$;
   $O_2 = O_3$;
   $||O_1|| = ||O_2||$

This particular procedure is the one implemented for the later K-complexity results in sections 7 and 8.

6.1.3 Re-orthogonalization procedures

The first method to deal with the loss of orthogonality due to numerical instability was put forward by Lanczos himself in his original work; Lanczos suggested repeated checking of orthogonality of the generated vectors, and subtracting off any residual [4]. This is a modification to a full (or modified) Gram-Schmidt (FGS) type procedure [5, 84], and is known as *Full Orthogonalization* (FO). Previously, at each Lanczos step, we subtracted off the projection onto the previous and current Krylov vector. For FO we subtract off the projection onto *all* previous Krylov vectors. The FO algorithm is given by:

1. $K_{-1} \equiv 0$
2. $b_0 \equiv 0$, $K_0 \equiv \mathcal{O}/||\mathcal{O}||$
3. $a_0 = (K_0|\mathcal{L}|K_0)$
4. For $n \geq 1 : Q_n = \mathcal{L}K_{n-1} - \sum_{m=0}^{n-1}(K_m|\mathcal{L}|K_{n-1})\, K_m$
5. $b_n = ||Q_n||$
6. If $b_n = 0$, stop
7. $K_n = Q_n/b_n$
8. $a_n = (K_n|\mathcal{L}|K_n)$
9. $n = n + 1$, and go to step 4

It is convention for the full Gram-Schmidt subtraction step (in step 4) to be performed twice per iteration.

Full re-orthogonalization (FO) is stable but extremely computationally wasteful, in both space and memory efficiency. This is because the FO performs re-orthogonalization on vectors which often do not require it. To address this, various Partial Re-orthogonalization (PRO) schemes have been developed, which generally aim to reduce the number of re-orthogonalization steps. A commonly used PRO, fully detailed in [55], performs a parallel process alongside the Lanczos recursion which tracks the numerical error and only performs re-orthogonalization when the error exceeds a specified tolerance. A similar alternative is the Implicitly Restarted Arnoldi Method (IRAM) such as the one implemented in ARPACK. In this approach the Arnoldi process runs for some fixed number of iterations, after which the residual vector is treated as a function of the initial Arnoldi vector. This new starting vector is run through an iterative process which forces the residual to converge to zero [86, 87].

In the Krylov complexity literature, FRO and PRO algorithms have been used extensively for high-dimensional systems [60, 88, 89]. As discussed in Section 4.1, large or infinite systems often require many Lanczos coefficients to accurately describe their dynamics, resulting in large numerical errors for later Lanczos iterations, necessitating re-orthogonalization along the way.

6.2 Return Amplitudes

Calculation of the algebraic return amplitudes were done using Mathematica. Recall that the return amplitude of an operator $\mathcal{O}$ under evolution of H is given by

$$(\mathcal{O}|\mathcal{O}(t)) \;=\; \mathrm{Tr}\left(\mathcal{O}^\dagger e^{-itH}\mathcal{O}e^{itH}\right) \;. \tag{6.2}$$

The calculation of the matrix exponential can be made orders of magnitude faster by diagonalizing the Hamiltonian first. Here we can rewrite the Hamiltonian as $H = PDP^{-1}$, where D is a diagonal matrix made from the eigenvalues of H, and P is a matrix where its columns are the eigenvectors of H. Using this, we can express the return amplitude as

$$(\mathcal{O}|\mathcal{O}(t)) \;=\; \left(\mathcal{O}|P^\dagger e^{-itD}(P^{-1})^\dagger\, \mathcal{O}\, P^{-1}e^{itD}P\right) \;. \tag{6.3}$$

With finite-precision input, the number of negligible terms which will appear grows exponentially with system size. This leads to excessive memory requirements for large system sizes, if these terms are not suppressed at various intermediary algebraic steps.

6.3 Recursive Probability Formula

Given a return amplitude $(\mathcal{O}|\mathcal{O}(t)) = \phi_0(t)$, and Lanczos coefficients a_n and b_n, we can find iteratively find the next probability amplitude, ϕ_{n+1}, using the recursive relation

$$\phi_{n+1} = (K_{n+1}|\mathcal{O}(t)) = \sum_{m=0}^{n+1} k_{m,n+1}\partial_t^m (K_0|\mathcal{O}(t)) \,, \tag{6.4}$$

$$k_{m,n+1} = \frac{ik_{m-1,n} - a_n k_{m,n} + b_n k_{m,n-1}}{b_{n+1}} \,, \tag{6.5}$$

where $K_0 = \mathcal{O}$. For exact arithmetic, the nested derivatives of the return amplitude become computationally expensive to handle. The derivatives can instead be evaluated (in parallel) at discrete time points to improve efficiency. For finite-precision numerical expressions of the return amplitude, it is important to track possible precision loss in the derivative step.

7 Open Boundary Conditions

In this section we examine the growth of operators under the evolution of transverse-field Ising model (TFIM) with open boundary conditions (OBC). We will explore the K-complexity of simple local spin operators, non-local spin operators, and operators which map to simple local fermionic operators of the Kitaev chain. Key features such as saturation value, initial growth, and the dependence on operator location and size will be crucial to addressing the Parker *et al.* hypothesis.

Note that the Jordan-Wigner transformation provides an exact map between the OBC TFIM and OBC Kitaev chain. Therefore, the growth of a fermionic operator in the Jordan-Wigner representation under the evolution of the OBC TFIM, can be directly interpreted as the growth of the corresponding fermionic operator under the evolution of the OBC Kitaev chain. Also note that the TFIM is set to criticality with $J = g = 1$ for all numerical results in Section 7 and Section 8, unless otherwise stated.

7.1 K-Complexity of fermionic operators

Single-site fermionic operators have Jordan-Wigner representations with varying degrees of non-locality, depending on their locations. Non-locality here is referring to the conventional notion of operator size: the number of non-identity matrices in the tensor product decomposition of the operator. In particular if we consider the representation of fermionic operators as

$$c_j^\dagger = \left(\bigotimes_{l=1}^{j-1} \sigma^z\right) \otimes \sigma^- \otimes \left(\bigotimes_{l=j+1}^{L} I\right), \tag{7.1}$$

we can see that operators representing fermions which are further along the chain (higher site value) have a larger operator size. Should operator growth increase with operator size, we would expect a correlation between the fermion location and operator growth.

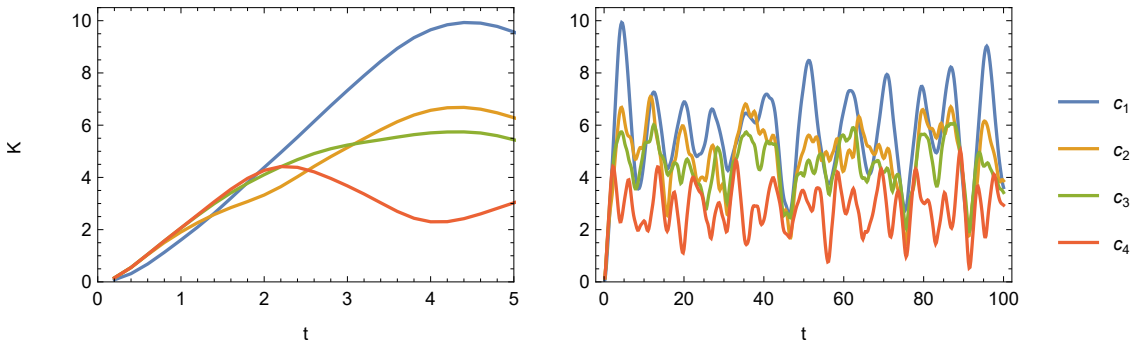

Figure 2. The early- and late-time K-complexity as a function of t of fermionic annihilation operators at sites 1 through 4. K-complexity is calculated with respect to the L=7 TFIM with OBC's. Operators at sites 5, 6, and 7 were omitted, as their K-complexities are identical to that of sites $3, 2, 1$ respectively.

Note that in Figure 2, the plots of K-Complexity of c_5, c_6, and c_7 operators were not included as they are identical to that of c_3, c_2, and c_1 respectively; this is due to the $\mathbb{Z}_2$ reflective symmetry. This symmetry can be intuitively thought of as arising from the ambiguity in the choice of whether the Jordan-Winger string should count the number of fermions starting from the left or starting from the right. More concretely, to map a local annihilation operator c_i to its reflected counterpart c_{L-i+1}, the following transformation can be done to its tensor product (Jordan-Wigner) representation: reflect the sites i.e. $i \to (L-i+1)$, then multiply by a full σ^z string i.e. $\bigotimes_{i=1}^{L} \sigma_i^z$ from the left. For instance, if $i = 2$,

$$\begin{aligned} c_2 \;&=\; \sigma^z \otimes \sigma^+ \otimes I \otimes \ldots \otimes I \\ &\qquad\qquad \downarrow \text{ flip} \\ &\qquad I \otimes \ldots \otimes I \otimes \sigma^+ \otimes \sigma^z \\ &\qquad\qquad \downarrow \text{ multiply by } \sigma^z \text{ string} \\ c_{L-1} \;&=\; \sigma^z \otimes \ldots \otimes \sigma^z \otimes \sigma^+ \otimes I \end{aligned}$$

Performing this transformation on an operator does not impact its dynamics w.r.t the PBC and OBC Ising Hamiltonian, since the σ^z string commutes with the Hamiltonian.

If we consider the very early-time[10] growth of c_1, c_2, and c_3 in Figure 2, there appears to be some correlation between increased operator size and the operator growth. However, this immediately gets contradicted if we consider the c_5, c_6, and c_7 operators—here we see a correlation between lower operator size and operator growth. The link between operator size and growth appears to be severed by the duality, lending support for the Parker *et al.* hypothesis.

7.2 Comparisons to local operators

The question which now naturally arises is: is the complexity of the large fermionic operators similar to that of small operators in the TFIM? Well, our choice of small operator matters significantly.

The local spin analog of the fermionic creation (annihilation) operators would be the spin raising (lowering) operators acting on site j. The spin raising operator on site j take the form

$$\sigma_j^+ \;=\; \left(\bigotimes_{l=1}^{j-1} I \right) \otimes \sigma^+ \otimes \left(\bigotimes_{l=j+1}^{L} I \right), \tag{7.2}$$

whose K-complexity will have a trivial $\mathbb{Z}_2$ end-to-end site-flip symmetry[11].

We begin by examining the site dependence of the local spin operators σ^+ and σ^x in figures 3 and 4 respectively. It is evident that the K-complexity is much larger for operators located closer to the centre of the chain, both at early and late times. This contrasts with

[10] We refer to the parameter t as time, which has units $1/J$. Early-time refers to values of t before the saturation time. The saturation time is a function of both the coupling and the Krylov dimension, and thus differs for each operator. We can describe it qualitatively as the time t where $K(t)$ first decreases.

[11] End-to-end site-flip symmetry refers to an invariance under the mapping of sites $j \leftrightarrow L - j + 1$.

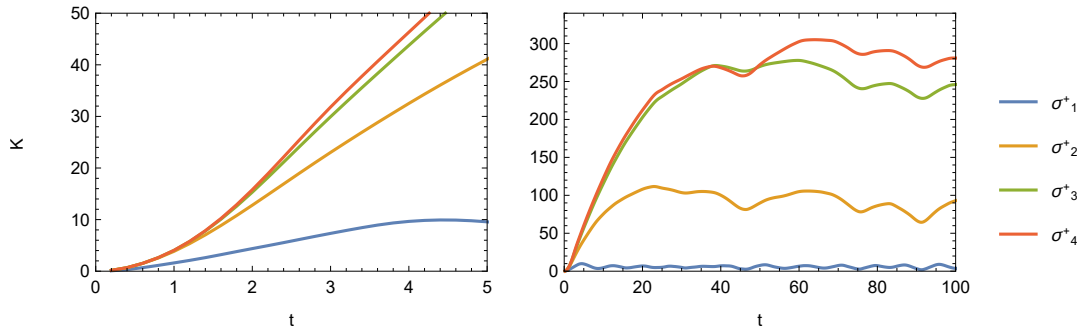

Figure 3. The early- and late-time K-complexity as a function of t of σ^+ operators at sites 1 through 4. K-complexity is calculated with respect to $L = 7$ TFIM with OBC's.

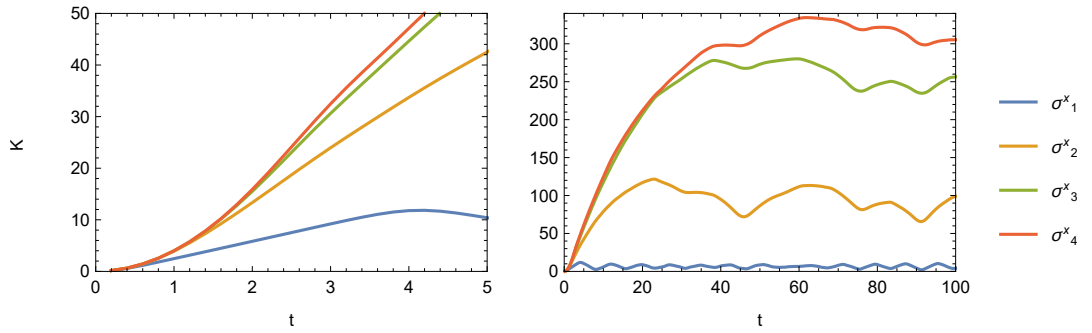

Figure 4. The early- and late-time K-complexity as a function of t of single site σ^x operators. K-complexity is calculated with respect to $L = 7$ TFIM with OBC's.

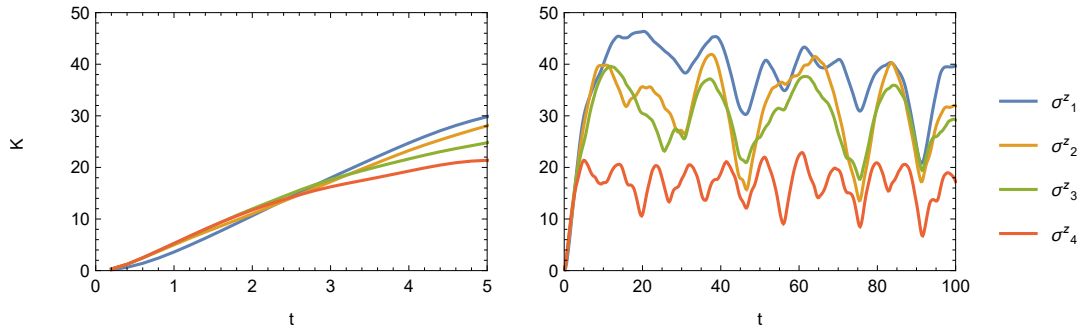

Figure 5. The early- and late-time K-complexity as a function of t of single site σ^z operators.n K-complexity is calculated with respect to $L = 7$ TFIM with OBC's.

the site-dependence of σ^z seen in Figure 5, where early time growth appears uniform across sites, while the late-time saturation value is lower at the centre of the chain.

This behaviour is easily understood in the fermionic picture. The σ_i^+, σ_i^x, and σ_i^y

operators have minimal fermionic representations which vary in size depending on their corresponding site. For example, under the IJW mapping we have $\sigma_1^+ \to c_1$, and $\sigma_2^+ \to c_1(1-2c_1^\dagger c_1)c_2$. If we account for the reverse ordering of the Jordan-Wigner string, we have the mapping $\sigma_L^+ \to_2 c_1$, and $\sigma_{L-1}^+ \to_2 c_1(1-2c_1^\dagger c_1)c_2$, where $\to_2$ represents the IJW with a site-reversed Jordan-Wigner string. Thus, the σ^+ and σ^x operators with the largest minimal fermionic representation are the operators nearest the centre of the chain.

Next, consider the site dependence of the saturation value. The evolution of the fermionic operator containing n on-site operators in the Kitaev chain is constrained to a subspace of dimension $\binom{2L}{n}$. This implies that the size of the Krylov subspace is bounded by this value, with the K-complexity saturation value roughly approximated by half the subspace size—this approximation holds well for systems exhibiting chaotic dynamics. Notably, the fermion operator subspace dimension, $\binom{2L}{n}$, correlates with the expected K-complexity saturation value. The σ^+ and σ^x operators closer to the centre have larger fermionic representations, and thus have a much larger evolution subspace. With far more space to explore, we expect a larger K-complexity saturation value. This matches the behaviour we observe in figures 3 and 4.

In contrast, the σ_i^z and c_i operators have the same fermionic representation size across all sites. Figures 2 and 5, show that this corresponds to their complexity saturation values being similar across different sites, except for those at the centre of the chain. The operators situated at the centre, σ_4^z and c_4, exhibit an additional reflective symmetry, and since the Hamiltonian has this symmetry too, their associated time-evolved counterparts, $\sigma_4^z(t)$ and $c_4(t)$, do as well. This reduces the size of the subspace containing their operator evolution, and so we expect lower K-complexity saturation values. A direct comparison of the saturation values of σ_i^z and c_i for fixed site i in figures 2 and 5 shows that the σ^z operators have significantly larger growth than c operators; this is due to their larger fermionic representation relative to c operators.

Now let's consider the early time growth. Figures 3 and 4 show that σ_i^+ and σ_i^x operators nearer the centre exhibit much faster early time growth. This correlates with the σ_i^+ and σ_i^x operators nearer the centre having a larger minimal fermionic representation. Meanwhile, figures 2 and 5 show that c_i and σ_i^z operators have very little site-dependence at early times, consistent with their equal fermionic representation sizes across sites. These observations indicate a strong correlation between the size of an operator in fermionic representation and the early-time growth of the operator's K-complexity.

7.3 Comparisons to large operators

The Jordan-Wigner representation of fermionic operators clearly have quite unique behaviour, but have similar site dependence to σ^z operators at both early and late times. Clarifying the cause of the fermionic operator's uniqueness requires us to try to tease out what aspects of its behaviour are due to its duality to local fermionic operators, and what can be attributed to its operator structure. To this end we can construct a set of operators with the same multi-site Jordan-Wigner representation as c_j, but with the string of σ^z

replaced with alternative Pauli matrices:

$$(c_x)_j = \left(\bigotimes_{l=1}^{j-1} \sigma^x\right) \otimes \sigma^+ \otimes \left(\bigotimes_{l=j+1}^{L} I\right) . \tag{7.3}$$

The spin representations of c_x and c thus have a similar non-local tensor product construction, but map to non-local and local fermionic operators respectively.

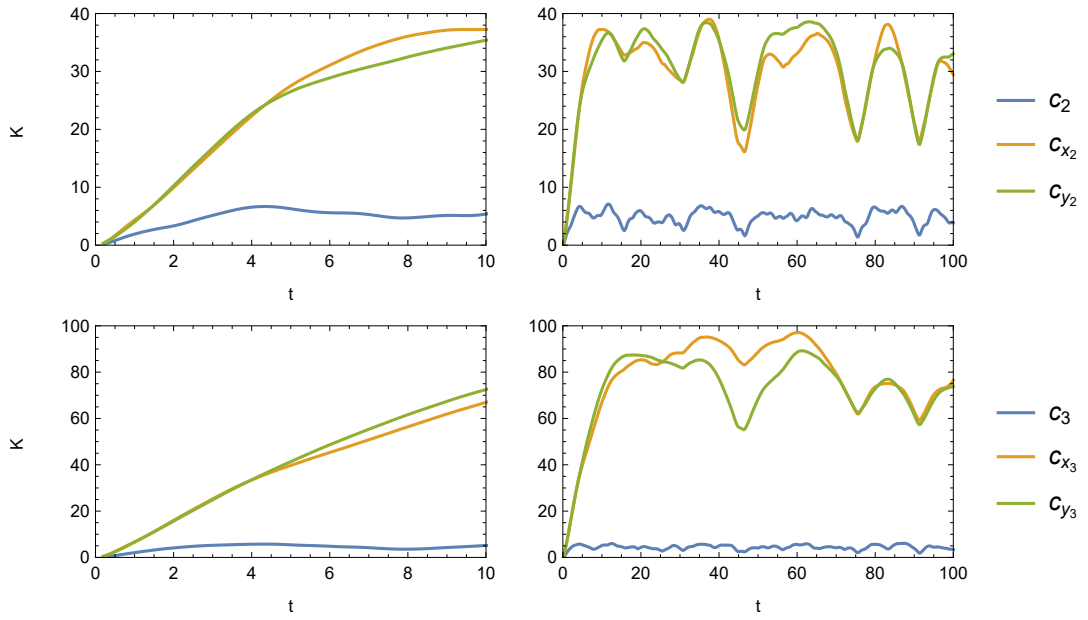

Figure 6. The early- and late-time K-complexity as a function of t of fermionic annihilation operators at sites 2 and 3, against the same operator construction with the σ^z Jordan-Wigner string replaced by σ^x and σ^y strings. K-complexity is calculated with respect to the $L = 7$ TFIM with OBC's.

From Figure 6 we can see that the fermionic operators c_j have quite different behaviour from the $(c_x)_j$ and $(c_y)_j$ operators. In particular, the c_j operators have an extremely low complexity saturation value, and a much lower initial growth. Furthermore, we can see that the saturation values of the fermionic operators have a completely different site-dependence.

We could also compare the complexity of the fermionic operators to other non-local operator constructions. A simple choice for non-local spin operators is simply to build larger operators out of σ^+ excitations. We will denote the multi-site operators using a shorthand where the subscripts of an operator denote the location along the product chain at which the operator lies, and all other sites will contain the Identity. For instance,

$$\sigma^+_{12} := \sigma^+ \otimes \sigma^+ \otimes I \otimes \ldots \otimes I \, . \tag{7.4}$$

The early and late time complexity of multi-site σ^+ operators are presented in Figure 7. Paying attention to the site dependence, we can see that the complexity saturation of the multi-site σ^+ is maximized for 4-site or 5-site operators, and minimized for the 1-site

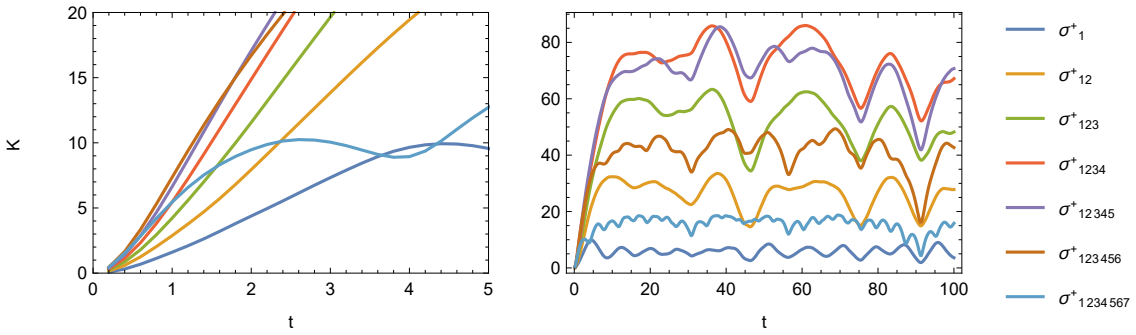

Figure 7. The early- and late-time K-complexity as a function of t of multi-site σ^+ operators. K-complexity is calculated with respect to the L=7 TFIM with OBC's.

and 7-site operator. This particular behaviour can be intuitively expected for multi-site operators built from the same excitation on multiple sites. This expectation arises from the combination of the following two points: The multiplicity of the set of operators that can be built from n identical on-site operators on the L site chain is maximized at $n = L/2$. The spin operators containing more identity operators will also expect less operator growth.

At early times in Figure 7 we see a strong correlation between these operators' size and their initial growth. This once again lends credence to the hypothesis: for simple spin operators, operator size is strongly linked to early time operator growth, but for the set operators that are dual to local fermionic excitations, operator size is uncorrelated to operator growth except at perhaps very early times.

8 Periodic Boundary Conditions

8.1 Twist effects seen by state complexity vs operator complexity

One of the key results of this work is that spread complexity is not sensitive to the break in symmetry caused by the Jordan-Wigner twist term, while operator complexity is. Briefly, spread complexity's indifference to the apparent symmetry break boils down to the fact that for any fixed state of definite fermionic parity, the Jordan-Wigner string has a fixed value, -1 or 1, whereas K-complexity as defined in this work uses an inner product which sums over states of both fermion parities, resulting in the Jordan-Wigner string evaluating to 1 for states in the even parity sector, and -1 for those in the odd parity sector. In this section we will discuss this in more detail.

Let us begin to unravel this by isolating the loose end—the stray Jordan-Wigner string in the boundary term of the Hamiltonian. Recall that the bulk terms of the TFIM Hamiltonian, H_{Ising}, and its dual H_{JW} have the form $\sigma_j^x\sigma_{j+1}^x \to (c_j^\dagger - c_j)(c_{j+1} + c_{j+1}^\dagger)$, whilst the boundary term is of the form

$$\begin{aligned}\sigma_L^x\sigma_1^x \;&\to\; \Big((1-2c_1^\dagger c_1)(1-2c_2^\dagger c_2)\dots(1-2c_{L-1}^\dagger c_{L-1})(c_L^\dagger + c_L)\Big)\,(c_1^\dagger + c_1) &(8.1)\\ &= S_L(c_L + c_L^\dagger)(c_1 + c_1^\dagger) &(8.2)\\ &= S_{L+1}(c_L - c_L^\dagger)(c_1 + c_1^\dagger) &(8.3)\end{aligned}$$

where $S_j = \exp\left(i\pi\sum_{i=1}^{j-1} c_i^\dagger c_i\right) = \prod_{i=1}^{j-1}(1-2c_i^\dagger c_i)$ is the Jordan-Wigner string operator, which simply counts the parity of the number of fermions on the chain strictly before site j. In other words, S_{L+1} acting on some state simply returns the parity of the total number of fermions in the state as an eigenvalue.

8.1.1 Boundary effects on state complexity

We would like to know what impact this term has on the symmetries of the observables in spread complexity. Consider the spread complexity of a time-evolved reference state $|\psi(t)\rangle$ under the evolution of the PBC Ising chain or its dual, H_{JW}. The dynamics encoded in the spread complexity is fully encoded in the return amplitude,

$$R(t) = \langle\psi|e^{-itH_{\text{JW}}}|\psi\rangle\ . \tag{8.4}$$

Consider the case in which $|\psi\rangle$ has an odd fermion parity. It follows that $S_{L+1} = -1$, and thus the boundary term takes the exact form of the bulk terms, i.e. $\sigma_L^x\sigma_1^x = (c_L^\dagger - c_L)(c_1 + c_1^\dagger)$. Thus, for $|\psi\rangle$ of odd parity H_{JW} is equivalent to the periodic Kitaev chain. This Hamiltonian is trivially invariant under any permutation of the site-indeces and therefore its dynamics are completely site-invariant. In other words, for some parity-odd localized operator $\hat{C}_i$ we have that

$$\langle\hat{C}_i|e^{-itH_{\text{JW}}}|\hat{C}_i\rangle \;=\; \langle\hat{C}_j|e^{-itH_{\text{JW}}}|\hat{C}_j\rangle \qquad \text{for } i \neq j\ , \tag{8.5}$$

where $|\hat{C}_j\rangle$ refers to the state corresponding the action of the $\hat{C}_j$ on the vacuum. This is a strong symmetry of the return amplitude; this restricts the operator growth to a very small subspace, resulting in a very low complexity saturation value.

Now consider the case where the number of fermions in $|\psi\rangle$ is even, here we have that $S_{L+1} = 1$, then $\sigma_L^x \sigma_1^x = -(c_L^\dagger - c_L)(c_1 + c_1^\dagger)$, and thus H_{JW} is equivalent to the anti-periodic Kitaev chain. The action of the Hamiltonian on some local operator will be the same everywhere except at the boundary, where the Hamiltonian's action differs by a minus sign. Note that the return amplitude of some local operator will not pick up a minus sign until the time evolution is at an order where the spread has fully wrapped around i.e. until it gets a winding contribution. All contributions to the return amplitude before the winding contribution would either not cross the boundary, or would have to cross it twice to get back—thus not picking up a minus sign.

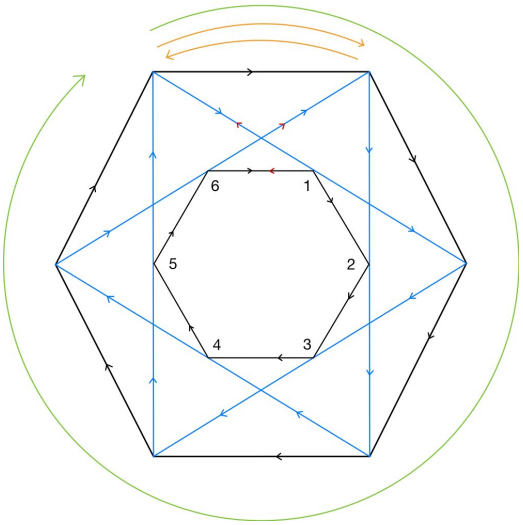

Figure 8. Illustration depicting creation and annihilation operators on a 6-site periodic chain. Let the black edges and blue edges represent particle hopping terms and superconducting terms respectively. All early contributions to the return amplitude will be of the form which does not cross the boundary, or crosses the boundary twice, represented by the orange arrow. After some time, we will get contributions which will pick up a winding factor, represented by the green arrow.

8.1.2 Boundary effects on operator complexity

Due to the nature of the chosen trace inner product, operator complexity exhibits completely different symmetry properties to state complexity. Recall that the Krylov complexity of a time-evolved operator, $\mathcal{O}(t)$, with respect to evolution under the PBC Ising chain or its dual H_{JW} is encoded in the return amplitude,

$$\phi_0(t) = (\mathcal{O}|\mathcal{O}(t)) = \text{Tr}(\mathcal{O}^\dagger e^{itL}\mathcal{O}) = \sum_n \langle n|\mathcal{O}^\dagger e^{itH_{\text{JW}}}\mathcal{O}e^{-itH_{\text{JW}}}|n\rangle \ . \tag{8.6}$$

This trace runs over all states—states which can have even or odd parity. If we consider the operator having odd parity, then a summand of the trace will then contain different projections of the Hamiltonian in each exponential. For example consider a localized parity-odd operator $\hat{C}_i$ in the even and odd summands of the trace. Here the only non-zero

summands will have the form:

$$\langle n_{\text{odd}}|\hat{C}_i^\dagger\ e^{itH_{\text{JW}}^+}\ \hat{C}_i\ e^{-itH_{\text{JW}}^-}|n_{\text{odd}}\rangle\ , \tag{8.7}$$

$$\langle n_{\text{even}}|\hat{C}_i^\dagger\ e^{itH_{\text{JW}}^-}\ \hat{C}_i\ e^{-itH_{\text{JW}}^+}|n_{\text{even}}\rangle\ . \tag{8.8}$$

Similarly, if we consider some parity-even operator $\hat{C'}_i^\dagger$, then the same projections of H_{JW} contribute to each summand,

$$\langle n_{\text{odd}}|\hat{C'}_i^\dagger\ e^{itH_{\text{JW}}^-}\ \hat{C'}_i\ e^{-itH_{\text{JW}}^-}|n_{\text{odd}}\rangle\ , \tag{8.9}$$

$$\langle n_{\text{even}}|\hat{C'}_i^\dagger\ e^{itH_{\text{JW}}^+}\ \hat{C'}_i\ e^{-itH_{\text{JW}}^+}|n_{\text{even}}\rangle\ . \tag{8.10}$$

We can see that for parity-even operators the summands contain the same Hamiltonian projection in each exponential. The summands corresponding to odd states can thus gain additional symmetries of periodicity, and even states that of anti-periodicity. Note that since the trace sums over both even and odd states the return amplitude—and thus the operator complexity—will lack periodic and anti-periodic symmetry. Nevertheless, since each of the summands of even parity operators are more restricted by additional symmetries than the odd parity operators, we will expect lower complexity for even parity operators than odd parity operators.

One less powerful symmetry which we can still expect from the operator growth of the local fermionic operators is a $\mathbb{Z}_2$ 'end-to-end' flip symmetry. This was shown in the OBC section and holds for the PBC case too.

8.2 Comparisons to local operators

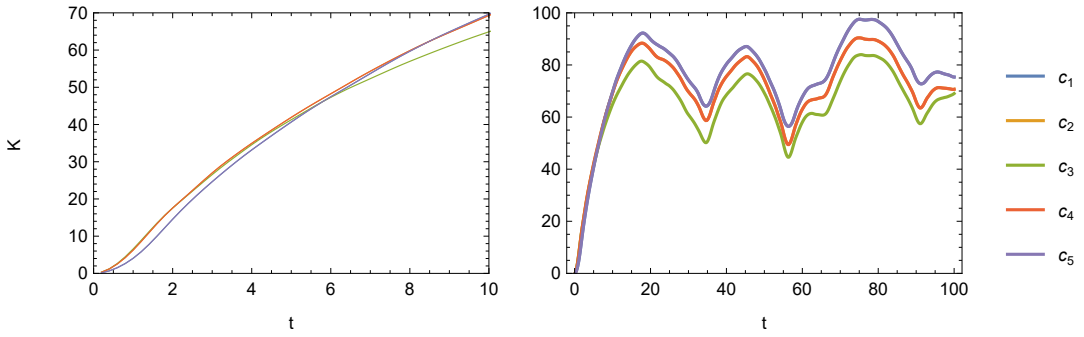

Figure 9. The early- and late-time K-complexity as a function of t of the creation operators at various sites. K-complexity is calculated with respect to $L = 5$ TFIM with PBC's. Note that the K-complexity of c_1 is exactly equivalent to that of c_5, and K-complexity of c_2 equivalent to that of c_4. Also note that K-Complexity of c_1 is exactly equivalent to that of all σ_j^+ due to the fact that $c_1 = \sigma_1^+$ and site-independence symmetry for the single-site σ^+ excitations.

Figure 9 offers a comparison between the growth of fermionic operators and local spin operators w.r.t the PBC Ising model, since c_1 is exactly σ_1^+ (and will have equivalent complexity to all σ_i^+ due to the site-independence symmetry). The behaviour of the single-site

fermionic and single-site spin operators is broadly similar, and they differ only in saturation value. A significant exception is evident with spin operators aligned to the magnetic field direction, as shown in Figure 10. In this figure, it is clear that spin operators aligned with the magnetic field direction exhibit significantly lower K-complexity, particularly at the saturation scale. Additionally, this figure shows that spin operators aligned with the interaction direction have the highest K-complexity saturation value.

Figure 9 shows a $\mathbb{Z}_2$ site flip symmetry. This is initially unintuitive, but is consistent with the argument presented in Section 7.1. In addition, we observe that operators positioned closer to the center of the chain display slightly lower complexity at late times and slightly higher complexity at early times. The K-Complexity in both the OBC and PBC case thus share similar overall structure, but have saturation values which differ by an order of magnitude. This is consistent with the analysis in Section 8.1.2, which argued that operator complexity on the PBC Ising chain will cause operators with odd fermionic parity to have much lower symmetry constraints, resulting in a much larger operator growth.

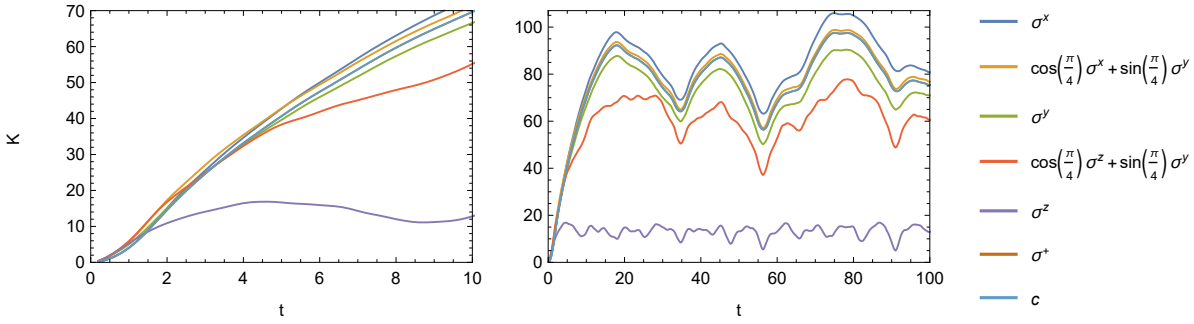

Figure 10. The early- and late-time K-complexity as a function of t of various combinations of Pauli operators on 1 site. K-complexity is calculated with respect to the $L = 5$ TFIM with PBC's, which has the ferromagnetic interaction in the σ^x direction, and the magnetic field direction of σ^z. Note that the complexity of σ^+ is equivalent to that of $\cos(\frac{\pi}{4})\sigma^x + \sin(\frac{\pi}{4})\sigma^y$

.

8.3 Comparisons to large operators

As in the OBC case before, we would like to compare the K-Complexity of the fermionic operators to a selection of multi-site operators. What we find is that the saturation value of the K-Complexity of the fermionic operators is in fact larger than that of most multi-site operators. This contrasts intuition carried over the OBC results.

In Figure 11 we compare the fermion annihilation operators to the $(c_x)_j$ and $(c_y)_j$ constructions which have a similar non-local structure, as described in Equation 7.3. The first notable observation is the breaking of the $\mathbb{Z}_2$ site-flip symmetry: $(c_x)_j$ and $(c_y)_j$ each have significantly different complexities for $j = 2$ and $j = 4$. As discussed in Section 7.1 that this $\mathbb{Z}_2$ symmetry arose from an invariance under the transformation that flips sites, $j \leftrightarrow L - j + 1$, and acts the operator $\bigotimes_{j=1}^{L} \sigma_i^z$ on the reference operator and Hamiltonian.

The absence of this symmetry for $(c_x)_j$ and $(c_y)_j$ stems from the fact that, unlike $\bigotimes_{i=1}^{L} \sigma_i^z$, the operators $\bigotimes_{i=1}^{L} \sigma_i^x$ and $\bigotimes_{i=1}^{L} \sigma_i^y$ do not commute with the Hamiltonian.

Another important observation from Figure 11 is that early-time growth correlates with operator size for $(c_x)_j$ and $(c_y)_j$, but does not correlate with operator size for c_j. However, it is evident that the K-complexity saturation value does not have the same correlation to operator size. Once again, going to the dual fermionic picture helps us understand. Under the Jordan-Wigner transformation the constructions of $(c_x)_i$ and $(c_y)_i$ have an even fermion parity for even site number i and an odd fermion parity for odd i. As previously discussed, under the evolution of H_{JW}, operators with even fermion parity are expected to have a significantly lower K-complexity saturation value compared to those with odd fermion parity, owing to the additional symmetries in the summands of the return amplitude that the former possess.

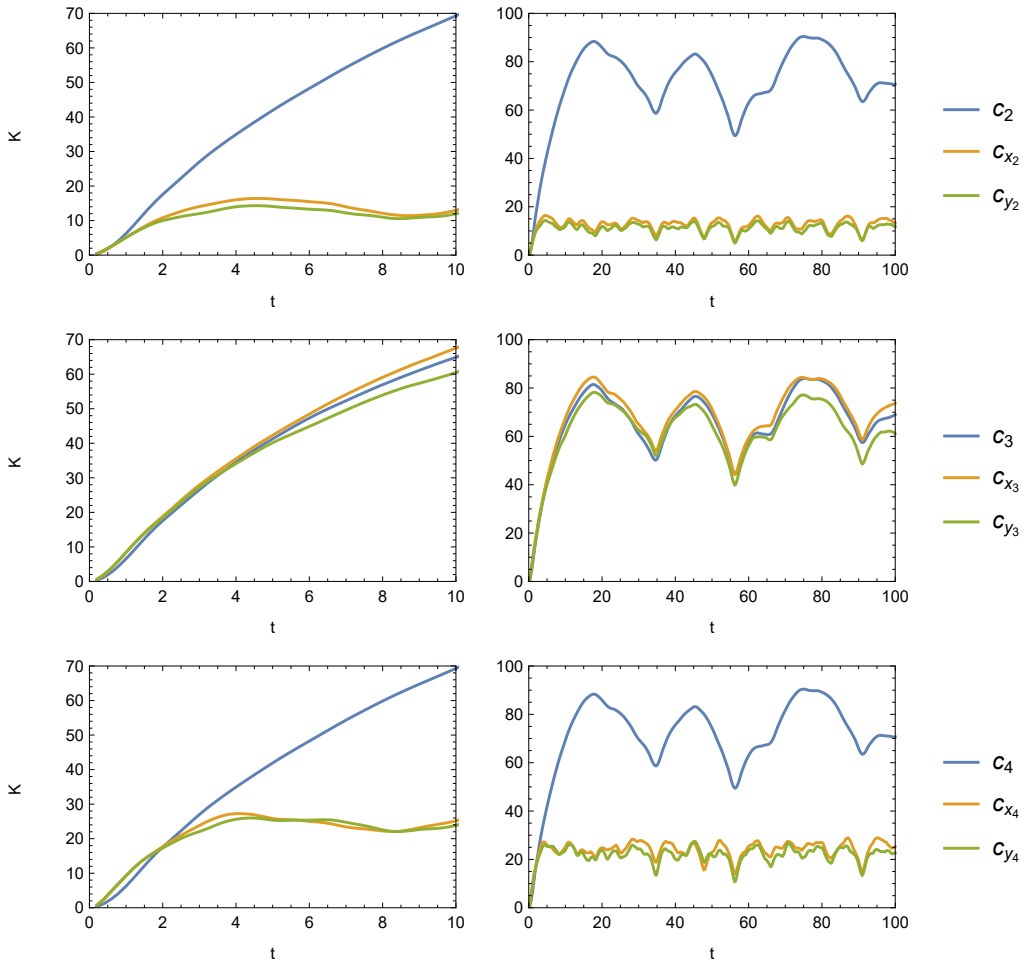

Figure 11. Early- and late-time K-complexity as a function of t of fermionic annihilation operators at sites 2, 3, and 4 against the same operator construction with the σ^z Jordan-Wigner string replaced by σ^x and σ^y strings. K-complexity is calculated with respect to the $L = 5$ TFIM with PBC's.

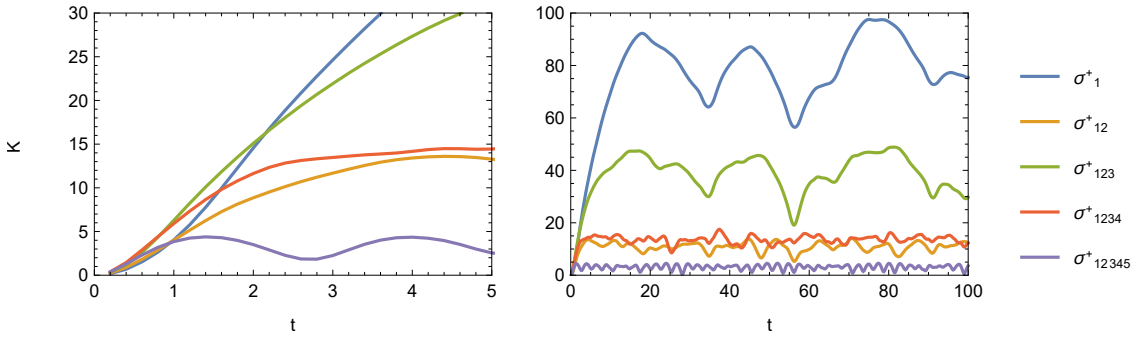

Figure 12. The early- and late-time K-complexity as a function of t of multi-site operators containing only σ^+'s. K-complexity is calculated with respect to the $L = 5$ TFIM with PBC's.

Figure 12 shows the complexity for non-local operators built out of σ^+ excitations as described in Equation 7.4. Noting that $\sigma^+_1 = c_1$, we can see that the complexity of the fermionic operators completely eclipses that of the multi-site σ^+ excitations. The low saturation complexity for σ^+_{12} and σ^+_{1234} follows simply: multisite σ^+ operators with even number of σ^+'s can be mapped to a parity even fermionic operator which—despite its non-locality—will still have a much lower complexity than a parity odd operator like c_i or σ^+_i. The early time growth in Figure 12 shows no clear correlation to operator size in the spin representation, nor in the corresponding fermionic representation.

8.4 Away from criticality

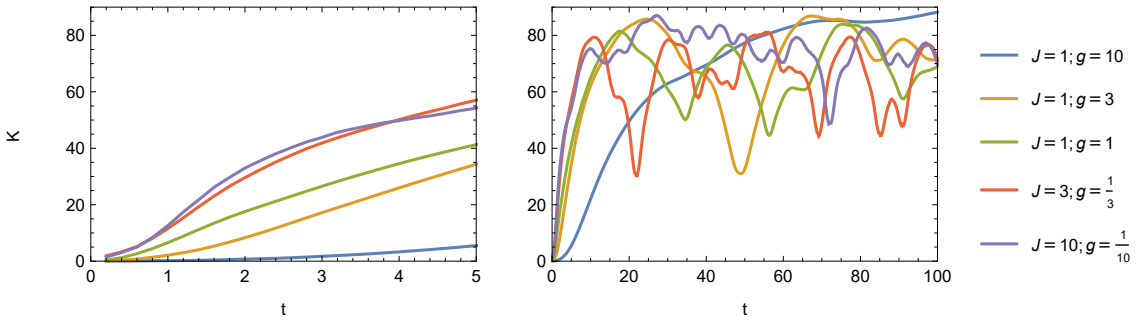

Figure 13. The early- and late-time K-complexity as a function of t of c_3 operator with respect to the $L = 5$ PBC TFIM, for various values of relative interaction strength, and the norm of the Hamiltonian is kept constant.

In Figure 13 we observe that the initial growth of the fermionic operators is proportional to the relative ferromagnetic interaction strength. Recall that under the duality, a larger ferromagnetic interaction strength corresponds to a larger particle-hopping coefficient and a larger superconducting coefficient. The superconducting terms allow the $c_3(t)$ access to sectors with other particle numbers within the odd parity sector. This accesses new, orthogonal spaces faster than exploring the sector of fixed particle number. The K-complexity

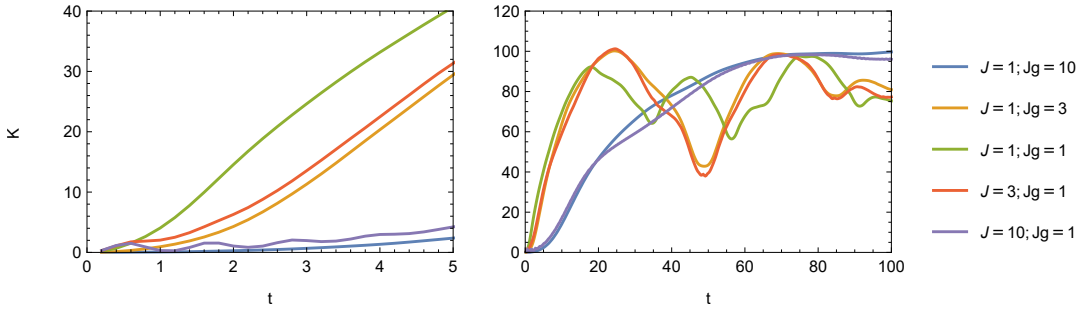

Figure 14. The early- and late-time K-complexity as a function of t of σ_3^+ operator with respect to the $L = 5$ PBC TFIM, for various values of relative interaction strength, and the norm of the Hamiltonian is kept constant.

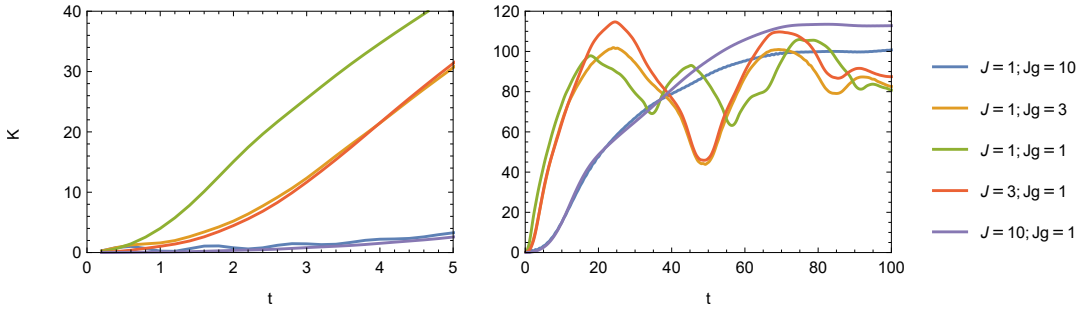

Figure 15. The early- and late-time K-complexity as a function of t of σ_3^x operator with respect to the $L = 5$ PBC TFIM, for various values of relative interaction strength, and the norm of the Hamiltonian is kept constant.

saturation values of the c_3 operators observed in Figure 13 are roughly equal. This is despite the spin phase transition, from the spin symmetric phase to the spin symmetry breaking phase. As outlined in Section 5.6, these phases of the TFIM both correspond to symmetric fermion phases, whose symmetry subspace have the same finite size.

In contrast to the coupling dependence of c_3, Figures 14 and 15 shows that the σ_3^+ and σ_3^x operators have initial growth that is highest at criticality, decreasing as the difference between the interaction strength and magnetic field strength increases. This is interesting behaviour that indicates the effect of some coupling symmetry where $J \leftrightarrow Jg$, such as Kramers-Wannier duality, but the exact mechanism is not apparent to us.

9 Conclusion

With open boundary conditions (OBCs), the Jordan-Wigner mapping between the Transverse field Ising Model (TFIM) and the Kitaev chain is exact. We find that operators that are large in the TFIM, but map to local operators in the Kitaev chain have very low K-complexity. The set of operators which map to local fermionic excitations vary in spin representation size without any correlation to operator growth. This example lends strong support to the Parker *et al.* hypothesis.

The Jordan-Wigner transformation maps the TFIM with periodic boundary conditions (PBCs) to a Hamiltonian, H_{JW}, which includes a non-local boundary twist term. H_{JW} is equivalent to the anti-periodic or the periodic Kitaev chain, depending on the fermion parity of the state upon which it acts, and thus can be split as the sum of two parts: the projections onto the even and odd parity sectors. The operator complexity utilizes both these projections, and thus exhibits fewer symmetries than had it only utilized one. Operators of odd parity are particularly affected, due to an additional loss of symmetry at the level of the summands of the trace in the return amplitude. This leads to a number of unintuitive consequences. The most notable is that simple operators such as c_i have very large K-complexity. The twist fundamentally alters the symmetries of the time-evolved operator, breaking down the correlation that we observed in the OBC case between operator size in fermionic representation and early-time K-complexity growth. We also intuitively expect the K-complexity of local fermionic operators like c_i to scale linearly with L, as it does in the OBC case, due to $c_i(t)$ remaining in the single excitation subspace. The Jordan-Wigner twist of the PBC allows $c_i(t)$ to explore the entire parity-odd sector; thus allowing the K-complexity to scale exponentially with L.

Studying the quantum XY model rather than the TFIM could provide a slightly more general look at the duality, as its Jordan-Wigner representation is the Kitaev chain without a constraint matching the superconducting strength to the hopping amplitude. This will allow for better exploration of the Kitaev chain parameter space. It has been shown that spread complexity can distinguish between topological phases of the Kitaev chain [41]. Reassessing this system through the Jordan-Wigner duality might provide further insight into the conditions under which spread complexity can be a diagnostic of topological phases transitions.

It is also crucial to note that, unlike for K-complexity, the growth of localized fermionic states observed by spread complexity exhibits a translational symmetry when imposing periodic boundary conditions. For any chosen reference state with a well-defined fermion parity, the return amplitude, $R(t) = \langle\psi|e^{itH_{\text{JW}}}|\psi\rangle$, will observe the projection of H_{JW} onto either the even or odd parity sector, where H_{JW} is the ABC or PBC Kitaev chain respectively. The insensitivity of spread complexity to phase information such as the Jordan-Wigner string at the boundary is a notable feature that warrants further attention.

Our OBC results showed that operator size tends to correlate to faster initial operator growth, but that this correlation completely breaks down when these spin operators map to local fermionic excitations. This indicates that the growth of an operator is mediated by its *simplest* description. This feels natural to a general notion of complexity—complexity is

measure of simplicity, it is a measure of the minimal required building blocks. However, we should be wary that this natural description does not obscure the subtleties of each system; we've seen that phase information at the boundary can break this relationship.

This natural description also does not explain why 'simple' operators of the Kitaev chain should have lower complexity than 'simple' operators of the Ising chain; this should be understood through the details of the symmetries and structure of the individual systems. In our context we saw that under the evolution of the Kitaev chain, fermionic operators explored the subspace of fixed particle number and constant parity in a neat ordering. This ordering gets mixed by the duality resulting in larger complexity on the spin side. It is also important to acknowledge that this effect is particular to integrable systems. Chaotic systems often have generic operator behaviour, with few exceptions, and thus bypass some of these subtleties of operator choice.

Although the Jordan-Wigner transformation is just one example, it serves as a foundation for the broader class of Bose-Fermi duality [39]. As a result, we expect that wrapping effects could lead to unintuitive impacts on operator growth in other dualities of this type. Further studies on related systems such as the 2D Ising CFT and its fermionic dual may offer clearer insights.

While progress has been made, much work remains in understanding how operator growth behaves across various dualities. Further studies are needed before we can fully harness the potential of complexity measures in making understanding these intricate dual systems a little less complex.

A State K-Complexity

State Krylov complexity, or spread complexity, was introduced in [54] as the K-complexity of a time-evolved reference state. In this section we will briefly outline how it is defined.

We can describe a time-evolved reference state in the Schrödinger picture as

$$|\psi(t)\rangle \;=\; e^{-itH}|\psi\rangle. \tag{A.1}$$

As for operator complexity, we can apply the Lanczos algorithm to orthogonalize the spanning set of the Krylov subspace of a state $\{|\psi\rangle, H|\psi\rangle, H^2|\psi\rangle, \ldots\}$. This produces the orthogonal Krylov basis, $\mathcal{K} = \{|K_i\rangle : i = 0, 1, 2 \ldots\}$, as well as two sets of Lanczos coefficients, $\{a_n : n = 0, 1, \ldots\}$ and $\{b_n : n = 1, 2, \ldots\}$.

In the Krylov basis the Hamiltonian takes on a tri-diagonal form

$$H|K_n\rangle = b_n|K_{n-1}\rangle + b_{n+1}|K_{n+1}\rangle + a_n|K_n\rangle \;, \tag{A.2}$$

We would like to describe the evolution of the reference state in terms of its spread along the Krylov basis. Simply expanding some time-evolved operator in terms of the Krylov basis we get the form of

$$|\psi(t)\rangle \;=\; \sum_n \phi_n(t)|K_n\rangle \;, \tag{A.3}$$

where this defines the probability amplitudes $\phi_n(t)$, and $|\phi_n(t)|^2$ describes the probability of the operator being in the n'th Krylov basis vector at time t. We can then write an expression for the evolution of the probability amplitudes in terms of the Lanczos coefficients,

$$i\partial_t\phi_n(t) \;=\; b_n\phi_{n-1}(t) + b_{n+1}\phi_{n+1}(t) + a_n\phi_n(t) \;. \tag{A.4}$$

This is the same discrete Schrödinger equation derived for the evolution of probability amplitudes of operator complexity. With knowledge of the Lanczos coefficients a_n and b_n, this equation allows us to solve for the time-evolved probability amplitudes, $\phi_n(t)$, using the initial condition $\phi_n(0) = \delta_{n,0}$.

Analogously to operator K-complexity, the state K-complexity of a time-evolved operator $|\psi(t)\rangle$, can then be defined as the weighted sum over the time-dependent probability amplitudes:

$$C_K(t) \;=\; \sum_n n|\langle K_n|\psi(t)\rangle|^2 \tag{A.5}$$

$$\;=\; \sum_n n|\phi(t)|^2 \;. \tag{A.6}$$

B Out-of-time-ordered Correlator

In a system with spatial locality, disturbances tend to propagate slowly, while systems with non-local interactions will induce a faster spread. Consider two localized observables represented by operators W and V. If they are localized on different sites, their operators commute, $[W, V] = 0$. When W is time-evolved, $W(t) = e^{iLt}W$, the operator may grow in size, and develop non-trivial support over sites upon which V has non-trivial support. In this scenario, measurement of the observables V and $W(t)$ become correlated, and the commutator $[W(t), V]$ will be non-vanishing. We can measure the growth of this non-commutation can be quantified with the commutator squared, commonly known as the *out-of-time-ordered* correlation function (OTOC),

$$\|[V, W(t)]\|^2 = ([V, W(t)][V, W(t)]) \ , \tag{B.1}$$

which contains contains a non-trivial component, which is commonly also referred to as the OTOC,

$$\langle V\, W(t)\, V\, W(t)\rangle \ . \tag{B.2}$$

These measures capture the ability of a system to scramble information and have become a standard probe of chaos [24, 25]. It was shown by [25] that OTOCs grow at most exponentially, $\sim e^{\lambda_L t}$ with the growth exponent bounded above by

$$\lambda_L \leq \frac{2\pi}{\beta} \tag{B.3}$$

where a regulated version of the thermal inner product was used. This is known as the MSS bound.

B.1 The OTOC is a Q-complexity

We begin by defining a superoperator resembling the Liouvillian, $\mathcal{L}_V \equiv [V, \cdot]$. Then for any operator $|W)$, we denote its action as $\mathcal{L}_V|W) = |[V, W])$. If we now define the Q operator as

$$\hat{Q}_{\text{OTOC}} = \mathcal{L}_V^2 \tag{B.4}$$

we see that the associated Q-complexity of some time-evolved operator $W(t)$ is simply the OTOC:

$$(W(t)|\hat{Q}_{\text{OTOC}}|W(t)) \ = \ (W(t)|\mathcal{L}_V^2|W(t)) \tag{B.5}$$

$\hat{Q}_{\text{OTOC}}$ is positive semi-definite, satisfying Equation 2.27. If we consider a k-local Hamiltonian and begin with localized operators W and V, the conditions 2.28 and 2.29 will naturally be satisfied too. Under these conditions, the OTOC is a Q-complexity and, as such, is bounded above by K-complexity. This relationship has been used to show that K-complexity growth can provide a tighter bound on the growth exponent than the MSS bound [26].

C More on the TFIM and Kitaev chain

C.1 Diagonalization of the Kitaev chain

We shall explore the exact solutions and critical limits of the Transverse Field Ising Model and its Jordan-Wigner dual Kitaev chain. The Kitaev chain is a simple quadratic system for which we can utilize the Bogoliubov-de-Gennes formalism to diagonalize and compute an exact spectrum [71].

In this section we will consider the Kitaev chain Hamiltonian with couplings consistent to the fermionic representation of the TFIM,

$$H_K = -\sum_j \left[J\left(c_{j+1}^\dagger c_j + c_j^\dagger c_{j+1}\right) \; - \; 2Jg\, c_j^\dagger c_j + g \; + \; J\left(c_j^\dagger c_{j+1}^\dagger + c_{j+1} c_j\right)\right] . \tag{C.1}$$

We begin, as all good math does, with a Fourier transform—in this case a discrete Fourier transform on lattice sites j,

$$c_j \; = \; \frac{1}{\sqrt{L}} \sum_k c_k e^{ijk_n} \; . \tag{C.2}$$

Here the allowed wavenumbers are

$$k_n = \frac{2\pi}{L}\left(-\left\lceil \frac{L-1}{2} \right\rceil + n + \frac{a}{2}\right) \; , \tag{C.3}$$

where we have $a = -1, 0, 1$ for anti-periodic, open, and periodic boundary conditions respectively. Note that in the case of odd L, or the case of even L and PBCs, k_n can take on values 0 or π. In either of these cases $c_k = c_{-k}$. We will consider $0 < k_n < \pi$, and consider these special cases later. For a thorough treatment of the Kitaev chain with general twisted boundary conditions, see [90].

We can now write the Fourier representation operators of the Hamiltonian with $0 < k = k_n < \pi$,

$$\begin{aligned}
\sum_j c_j c_{j+1} \; &= \; \sum_j \frac{1}{L} \sum_k c_k e^{-ijk} \sum_{k'} c_{k'} e^{-i(j+1)k'} && \text{(C.4)} \\
&= \; \sum_j \frac{1}{L} \sum_k c_k e^{-ijk} \sum_{k'} c_{k'} e^{-ijk'} e^{-ik'} && \text{(C.5)} \\
&= \; \frac{1}{L} \sum_k \sum_{k'} c_k c_{k'} e^{-ik'} \sum_j e^{-ijk} e^{-ijk'} && \text{(C.6)} \\
&= \; \sum_k c_k c_{-k} e^{ik} && \text{(C.7)}
\end{aligned}$$

where in the last line we used the Fourier representation of the Kronecker delta to collapse

the j sum. Similarly, we can express rewrite the other terms of the Hamiltonian

$$\sum_j c_j^\dagger c_{j+1}^\dagger = \sum_k c_k^\dagger c_{-k}^\dagger e^{-ik} \tag{C.8}$$

$$\sum_j c_j^\dagger c_{j+1} = \sum_k c_k^\dagger c_k e^{-ik} \tag{C.9}$$

$$\sum_j c_j c_{j+1}^\dagger = \sum_k c_k^\dagger c_k e^{ik} \tag{C.10}$$

$$2g\sum_j c_j^\dagger c_j = 2g\sum_k c_k^\dagger c_k \tag{C.11}$$

Combining this we get the Fourier transformed Hamiltonian,

$$H_F = -J\sum_k \left[c_k c_{-k} e^{ik} + c_k^\dagger c_{-k}^\dagger e^{-ik} + c_k^\dagger c_k e^{-ik} + c_k^\dagger c_k e^{ik} - 2g c_k^\dagger c_k + g\right] \tag{C.12}$$

The first two terms of C.12 can be simplified as

$$\sum_k c_k c_{-k} e^{ik} + c_k^\dagger c_{-k}^\dagger e^{-ik} \tag{C.13}$$

$$= \sum_k \left[\frac{1}{2}(c_k c_{-k} e^{ik} + c_k^\dagger c_{-k}^\dagger e^{-ik}) - \frac{1}{2}(c_{-k} c_k e^{ik} + c_{-k}^\dagger c_k^\dagger e^{-ik})\right] \tag{C.14}$$

$$= -\sum_k \frac{1}{2}(c_k c_{-k} e^{ik} + c_k^\dagger c_{-k}^\dagger e^{-ik}) - \sum_k \frac{1}{2}(c_{-k} c_k e^{ik} + c_{-k}^\dagger c_k^\dagger e^{-ik}) \tag{C.15}$$

$$= -\sum_k \frac{1}{2}\left[e^{-ik}(c_{-k} c_k + c_{-k}^\dagger c_k^\dagger) - e^{ik}(c_{-k}^\dagger c_k^\dagger + c_{-k} c_k)\right] \tag{C.16}$$

$$= -\sum_k \frac{1}{2}(c_{-k} c_k + c_{-k}^\dagger c_k^\dagger) 2i\sin(k) \tag{C.17}$$

$$= -i\sum_k \sin(k)(c_{-k} c_k + c_{-k}^\dagger c_k^\dagger) \tag{C.18}$$

where in the second we used the anti-commutation properties, and the third line we did a variable re-labelling $k \to -k$ for the first sum. The third and fourth terms of C.12 can be simplified more easily as

$$c_k^\dagger c_k e^{-ik} + c_k^\dagger c_k e^{ik} = 2\cos(k) c_k^\dagger c_k \tag{C.19}$$

This gives as the neat form

$$H_F = \sum_{\substack{k_n \\ k_n \neq 0,\pi}} \left[\left(2gJ - 2J\cos(k) c_k^\dagger c_k\right) + iJ\sin(k)\left(c_{-k} c_k + c_{-k}^\dagger c_k^\dagger\right) - Jg\right] \tag{C.20}$$

We now briefly acknowledge the cases which result in $k = 0$ and $k = \pi$. Splitting up the four cases, we can write the full Fourier transformed Hamiltonian, H_F', as [90]

$$H_F' = H_F + \begin{cases} 0 & (L = \text{even,APBC}) \\ H_F(0) + H_F(\pi) & (L = \text{even,PBC}) \\ H_F(\pi) & (L = \text{odd,APBC}) \\ H_F(0) & (L = \text{odd,PBC}) \end{cases} \tag{C.21}$$

where the contributions Hamiltonian contributions for $k = 0$ and $k = \pi$ are,

$$H_F(0) = -(2Jg - 2J)(a_0^\dagger a_0 - a_0 a_0^\dagger) \,, \tag{C.22}$$
$$H_F(\pi) = -(2Jg + 2J)(a_\pi^\dagger a_\pi - a_\pi a_\pi^\dagger) \,. \tag{C.23}$$

The Hamiltonian modes given by C.22 and C.23 are already diagonal. We will now proceed with diagonalizing H_F, C.20.

Dropping the constant term, Equation C.20 can be rewritten in the Bogoliubov-de Gennes (BdG) form. This is a re-expression of the Hamiltonian in the form $H = \Psi^\dagger H_{\text{BdG}} \Psi$ where Ψ is a vector of creation and annihilation operators, known as a Nambu spinor [79]. H_F in BdG form is given by,

$$H_F = J \sum_k \Psi_k^\dagger \begin{pmatrix} g - \cos(k) & -i \sin(k) \\ i \sin(k) & -g + \cos(k) \end{pmatrix} \Psi_k \,, \tag{C.24}$$

where $\Psi_k = \begin{pmatrix} c_{-k} \\ c_k^\dagger \end{pmatrix}$. We have effectively reduced C.1 to a 2×2 matrix H_{BdG} in the 'particle-hole' space. The matrix can then be diagonalized by performing a rotation, mixing the particle and hole sectors. This reformulatation of the Hamiltonian in terms of 'quasi-particle' variables which are superpositions of particles and holes, and is known as a *Bogoliubov transformation*. We start by defining the Bogoliubov quasi-particles, or *Bogoliubons*, γ_k,

$$\gamma_k \coloneqq u_k c_k - i v_k c_{-k}^\dagger \,, \tag{C.25}$$

where u_k and v_k satisfy

$$u_k^2 + v_k^2 = 1 \,, \tag{C.26}$$

as well as $u_{-k} = u_k$ and $v_{-k} = -v_k$ [73]. A convenient choice satisfying this is

$$u_k = \cos\left(\frac{\theta_k}{2}\right) v_k = \sin\left(\frac{\theta_k}{2}\right) \,, \tag{C.27}$$

where $\theta_k = \arctan\left(\frac{\sin(k)}{g - \cos(k)}\right)$. Substituting all c_k in C.20 we arrive at the diagonalized form of the Hamiltonian in terms of Bogoliubons,

$$H = \sum_k \Lambda_k \left(\gamma_k^\dagger \gamma_k - \frac{1}{2}\right) \,, \tag{C.28}$$

with the energy spectrum

$$\Lambda_k = 2J\sqrt{1 + g^2 - 2g\cos(k)} \,. \tag{C.29}$$

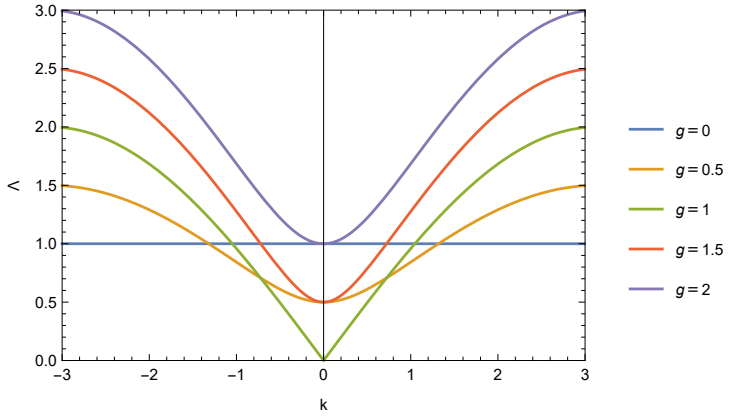

Figure 16. The energy spectrum Λ_k for various values of the coupling g. We can see the energy gap vanish at $g = 1$.

C.2 At criticality

In the low energy limit, the energy spectrum is approximately

$$\Lambda_k = 2J\sqrt{(1-g)^2 + gk^2} \tag{C.30}$$

At the critical point $g = g_c = 1$ we see that the energy gap vanishes, $\Lambda_k = 2J|k|$. Notice that in the low energy limit, the BdG Hamiltonian can be re-written in terms of Pauli matrices,

$$H_{\text{BdG}}(k) \approx \begin{pmatrix} g-1 & -ik \\ ik & 1-g \end{pmatrix} = J(g-1)\sigma^z + Jk\sigma^y \ . \tag{C.31}$$

Squinting our eyes, we can identify the Dirac physics emerging with a mass of $m = J(g-1)$, $H_{\text{Dirac}} = m\sigma^z + Jk\sigma^y$. In the massless limit (the critical point), this free fermionic theory becomes conformally invariant.

C.3 Majorana modes and their application to quantum computing

A Majorana 'fermion' is a quasi-particle excitation defined in terms of the fermionic creation and annihilation operators c and $c^\dagger$ as,

$$c^\dagger = \frac{1}{\sqrt{2}}(a + ib) \ , \tag{C.32}$$

$$c = \frac{1}{\sqrt{2}}(a - ib) \ , \tag{C.33}$$

such that each Majorana fermion is its own anti-particle i.e. $a = a^\dagger$. These obey the relations $\{a_j, a_k\} = 2\delta_{j,k}$, $\{b_j, b_k\} = 2\delta_{j,k}$, $\{a_j, b_k\} = 0$. Many believe that Majorana fermions are strong candidates for creating fault-tolerent qubits.

There are two primary causes the decoherence of qubits [79]: First, energy decay can cause classical bit flip errors and dephasing. The latter describes the process whereby the

relative phases between states are smeared out. Second, the operators acting on the qubits have small errors which accumulate over repeated application.

A relatively simple way to reduce bit-flip errors is by encoding the bits with the fermions, which can have occupied or unoccupied sites. The only way for a bit flip error to occur is if it happens at two sites simultaneously, due to charge conservation. By then placing the two sites controlling a qubit spatially far apart, we reduce the change of this occurring. The dephasing of these fermionic bits are still a concern—the occupation number of some qubit may fluctuate due to environment or measurement interactions. Kitaev introduced the idea that splitting each fermionic site into two Majorana modes, which can then be spatially separated, can mitigate dephasing. In particular, we hope to physically separate the Majorana modes γ_{2j} and γ_{2j-1} that together comprise the fermion number operator $c_j^\dagger c_j = (1+ia_{2j-1}a_{2j})/2$. This would mitigate phase errors, and altogether make this Majorana qubit immune to decoherence [79].

Majorana particles appear as quasi-particle excitations in certain superconducting systems such as the Kitaev chain. Recall the Kitaev chain Hamiltonian

$$H_{\text{Kitaev}} = \sum_{j=1}^{L}\left[-\frac{t}{2}\left(c_{j+1}^\dagger c_j + c_j^\dagger c_{j+1}\right) + \frac{\Delta}{2}\left(c_j^\dagger c_{j+1}^\dagger + c_{j+1}c_j\right)\right] - \sum_{j=1}^{L}\mu c_j^\dagger c_j \,, \tag{C.34}$$

can be written in terms of Majorana modes as

$$H_m = iJ\sum_j (a_j b_{j+1} - a_{j+1}b_j + g a_j b_j) \,, \tag{C.35}$$

up to constant factors, and with neglecting constant terms. We can see here that the in the $g \gg 1$, the dominant term is the one coupling Majorana modes at the same fermionic lattice site. This is known as the trivial phase. In the $g \to 0$ limit, we have the coupling Majorana modes of neighbouring fermionic lattice sites. This leaves unpaired Majorana modes on the ends of the chain, see Figure 17. These unpaired Majorana modes at the edge are known as *Majorana Zero Modes* (MZMs). Using the MZMs we can now write a new fermionic operator $\tilde{a} = \frac{1}{2}(a_1 + ib_L)$, where L is the length of the fermion chain. This operator can be used to define a 'qubit basis', with $\tilde{a}|0\rangle = 0$ and $\tilde{a}^\dagger|0\rangle = |1\rangle$.

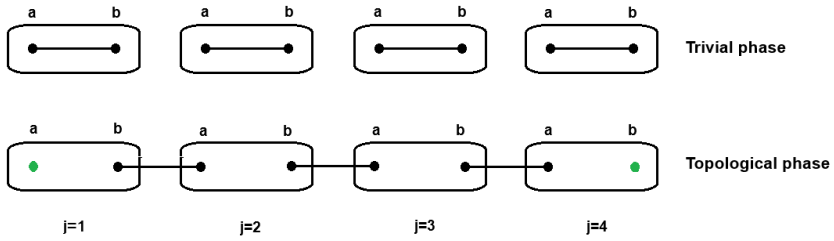

Figure 17. Diagrammatic representation of the pairing arrangements for Majorana modes in the Kitaev chain. The fermionic sites are labelled as $j = 1, 2, 3, 4$, with each site containing two Majorana modes, a and b. In the trivial phase, $g \gg 1$, the Majorana modes within each fermionic site are paired. In the topological phase, $0 \leq g \ll 1$ the Majorana modes couple across adjacent sites, leaving unpaired Majorana modes at each end.

D Canonical commutation relations

Suppose we have some set of operators $c_1, \ldots, c_n$ acting on some Hilbert space $\mathcal{H}_F$. These operators satisfy the canonical commutation relations for fermions if they satisfy

$$\{c_i, c_j^\dagger\} = \delta_{jk} I \tag{D.1}$$

$$\{c_i, c_j\} = 0 \, . \tag{D.2}$$

We will proceed in thinking of the CCRs as simply a set of mathematical conditions which define a set of operators. The important question to now ask is, what are the consequences of the operators satisfying CCRs? Do the resulting operators produce useful structures?

Following [68], we will present the mathematical consequences of imposing CCRs on some finite number of operators $c_1, \ldots, c_L$.

Operators $c_j^\dagger c_j$ are positive Hermitian operators with eigenvalues 0 and 1, since $(c_j^\dagger c_j)^2 = 0$. The operators c_j and $c_j^\dagger$ act as lowering and raising operators[12] respectively on the eigenstates of $c_j^\dagger c_j$. There exists a state $|\psi\rangle$ which is a simultaneous eigenstate for all $c_j^\dagger c_j$ operators, and by acting on ψ with all 2^L combinations of $c_1, \ldots, c_L$ and $c_1^\dagger, \ldots, c_L^\dagger$ operators, we construct a set of 2^L orthogonal states, ζ. Since all states in ζ are simultaneous eigenstates of $c_j^\dagger c_j$, each state in the set is uniquely labelled by its corresponding vector of eigenvalues. Let W be the subspace of $\mathcal{H}_F$ which is spanned by ζ, and $W_\perp$ be the orthocomplement of W in $\mathcal{H}_F$. We know exactly the action of c_j and $c_j^\dagger$ on W, that they map W onto itself. We can then show that c_j and $c_j^\dagger$ maps $W_\perp$ into itself, and identify a 2^L subspace of $W_\perp$ on which we know the action of c_j and $c_j^\dagger$. We can see now that we can iterate this procedure, and that if $\mathcal{H}_F$ is finite dimensional then this process terminates when the next orthocomplement in the iteration is the trivial vector space. When this process terminates, we will have partitioned the $\mathcal{H}_F$ into some finite number of orthogonal subspaces $W_1, W_2, \ldots, W_d$. Each of these vector spaces will be 2^L-dimensional and will have an orthonormal basis ζ.

[12]The operator c_j acting as a lowering operator means that for the eigenstate of $c_j^\dagger c_j$ with eigenvalue 0,

We can now represent the vector space V in a neat way. We can write down an orthonormal basis of vectors denotes $|\alpha, w\rangle$, where $w = 1, \ldots, d$ and α enumerates all 2^L states corresponding to w by running over the unique eigenvalue vectors (or neatly, all n-bit vectors). The action of c_j and $c_j^\dagger$ leaves w invariant. Here we can see that we are representing V as a tensor product $C^{2^n} \otimes C^d$. This is known as the *occupation number representation.*

E More on inner products

If we define the thermal expectation value

$$\langle A \rangle_\beta = \frac{\mathrm{Tr}(e^{-\beta H} A)}{\mathrm{Tr}(e^{-\beta H})} \,, \tag{E.1}$$

where $\beta = 1/T$, we can write a more general family of inner products that allow us to include finite temperature,

$$(A|B)_\beta^g \;=\; \int_0^\beta g(\lambda) \langle e^{\lambda H} A^\dagger e^{-\lambda H} B \rangle_\beta \, d\lambda \,. \tag{E.2}$$

Here we require that

$$g(\lambda) \geq 0, \qquad g(\beta - \lambda) = g(\lambda), \qquad \frac{1}{\beta} \int_0^\beta g(\lambda) d\lambda = 1. \tag{E.3}$$

Making the choice of $g(\lambda) = \delta(\lambda - \beta/2)$, we arrive as the standard Wightman inner product

$$(A|B) \;=\; \langle e^{H\beta/2} A^\dagger e^{-H\beta/2} B \rangle_\beta \,, \tag{E.4}$$

for which the infinite temperature limit is the Frobenius inner product $(A|B) = Tr(A^\dagger B)$. The Wightman inner product corresponds to taking the expectation value of the operators in a thermofield double state, where operators A and B are inserted into the two copies [33]. It has been shown that if we have solved for the dynamics using one specific choice for the inner product, that the behaviour for all other choices of inner product within our defined class can be found [33, 91].

$|0\rangle$, we have that $c_j|0\rangle = 0$, and for the eigenstate of $c_j^\dagger c_j$ with eigenvalue 1, $|1\rangle$, $c_j|1\rangle = |1\rangle$. Similarly, $c_j^\dagger$ acting as a raising operator means that we have that $c_j^\dagger|1\rangle = 0$, and $c_j^\dagger|0\rangle = |1\rangle$.

F Proofs

F.1 Unitary symmetry in complexity of time-evolved reference state

Theorem 3 *Suppose we have some unitary symmetry of the Hamiltonian, U, meaning that $U^\dagger U = 1$ and $U^\dagger H U = H$, and thus $[H, U] = 0$. If we transform the reference state, $|\mathcal{O}) \mapsto |\mathcal{O}') = U|\mathcal{O})$ then*

$$\mathcal{K}'_D = \mathcal{K}_D \tag{F.1}$$
$$|K'_n) = U|K_n) \qquad \forall n = 0, \dots, K-1 \tag{F.2}$$
$$a'_n = a_n \qquad \forall n = 1, \dots, K-1 \tag{F.3}$$
$$b'_n = b_n \qquad \forall n = 0, \dots, K-1 \tag{F.4}$$

Proof: The following is a simple proof of the theorem via strong induction on the Arnoldi iteration.
Base Case: We begin with the Arnoldi algorithm using the Hamiltonian H' and the reference operator $U|\mathcal{O}) = U^\dagger \mathcal{O} U$. As always we have that $K'_{-1} = K_{-1} = 0$, $b'_0 = b_0 = 0$. Since for any operator X, we have $\|U^\dagger X U\| = \|X\|$, and

$$[U^\dagger H U, U^\dagger X U] = U^\dagger [H, X] U \tag{F.5}$$

we immediately get the rest of the base case

$$K'_0 = U^\dagger \mathcal{O} U / \|\mathcal{O}\| = U^\dagger K_0 U \tag{F.6}$$
$$a'_0 = (K'_0|\mathcal{L}'|K'_0) = \mathrm{Tr}\left((U^\dagger \mathcal{O}^\dagger U)(U^\dagger [H, \mathcal{O}] U)\right) = a_0 \tag{F.7}$$

where in the last line we used $U^\dagger U = 1$ and the cyclic identity of the trace.
Inductive step: Assume that for all $n \leq m$

$$|K'_n) = U|K_n) \qquad \forall n = 0, \dots, K-1 \tag{F.8}$$
$$a'_n = a_n \qquad \forall n = 1, \dots, K-1 \tag{F.9}$$
$$b'_n = b_n \qquad \forall n = 0, \dots, K-1 \tag{F.10}$$

Now we show that it holds for $n = m+1$, starting with the intermediary variable Q_n for convenience.

$$Q'_{m+1} = [H', K'_m] - a'_m K'_m - b'_m K'_{m-1} \tag{F.11}$$
$$= U^\dagger [H, K_m] U - a_m U^\dagger b_{n+1} U^\dagger K_{n-2} U \tag{F.12}$$
$$= U^\dagger Q_{m+1} U \tag{F.13}$$

$$b'_{m+1} = \|Q'_{m+1}\| \tag{F.14}$$
$$= \mathrm{Tr}\left(U^\dagger Q^\dagger_{m+1} U U^\dagger Q_{m+1} U\right) \tag{F.15}$$
$$= b_{m+1} \tag{F.16}$$

$$K'_{m+1} = Q'_{m+1}/b'_{m+1} \tag{F.17}$$
$$= (U^\dagger Q_{m+1} U)/b_{m+1} \tag{F.18}$$
$$= U^\dagger K_{m+1} U \tag{F.19}$$

$$a'_{m+1} = \mathrm{Tr}\left((U^\dagger K^\dagger_{m+1} U)(U^\dagger [H, K_{m+1}] U)\right) \tag{F.20}$$
$$= \mathrm{Tr}\left(K^\dagger_{m+1}[H, K_{m+1}]\right) \tag{F.21}$$
$$= a_{m+1} \tag{F.22}$$

We have thus shown by strong induction that under simultaneous unitary transformations of the Hamiltonian and the reference operator, the Lanczos coefficients are invariant while the Krylov vectors transform as $|K_n) \mapsto U|K_n)$.

References

[1] B. Fauseweh, *Quantum many-body simulations on digital quantum computers: State-of-the-art and future challenges*, *Nature Communications* **15** (2024) 2123.

[2] V. Mukherjee and U. Divakaran, *The promises and challenges of many-body quantum technologies: A focus on quantum engines*, *Nature Communications* **15** (2024) 3170.

[3] T. Ayral, P. Besserve, D. Lacroix and E.A. Ruiz Guzman, *Quantum computing with and for many-body physics*, *The European Physical Journal A* **59** (2023) 227.

[4] C. Lanczos, *An iteration method for the solution of the eigenvalue problem of linear differential and integral operators*, *J. Res. Natl. Bur. Stand. B* **45** (1950) 255.

[5] G.M.D. Corso, O. Menchi and F. Romani, *Krylov subspace methods for solving linear systems*, .

[6] J.K. Cullum and R.A. Willoughby, *Lanczos Algorithms for Large Symmetric Eigenvalue Computations*, Classics in Applied Mathematics, Society for Industrial and Applied Mathematics (Jan., 2002), 10.1137/1.9780898719192.

[7] J. Liesen and Z. Strakos, *Krylov Subspace Methods*, in *Krylov Subspace Methods: Principles and Analysis*, J. Liesen and Z. Strakos, eds., p. 0, Oxford University Press (2012), DOI.

[8] L. Komzsik, *The Lanczos Method*, Software, Environments, and Tools, Society for Industrial and Applied Mathematics (Jan., 2003), 10.1137/1.9780898718188.

[9] Z.-Z. Bai, *Motivations and realizations of Krylov subspace methods for large sparse linear systems*, *Journal of Computational and Applied Mathematics* **283** (2015) 71.

[10] V.S. Viswanath and G. Müller, *The Recursion Method: Application to Many-Body Dynamics*, vol. 23 of *Lecture Notes in Physics Monographs*, Springer, Berlin, Heidelberg (1994), 10.1007/978-3-540-48651-0.

[11] D.C. Mattis, *How to Reduce Practically Any Problem to One Dimension*, in *Physics in One Dimension*, J. Bernasconi and T. Schneider, eds., (Berlin, Heidelberg), pp. 3–10, Springer, 1981, DOI.

[12] H. Mori, *A Continued-Fraction Representation of the Time-Correlation Functions*, *Progress of Theoretical Physics* **34** (1965) 399.

[13] P. Grigolini, G. Grosso, G.P. Parravicini and M. Sparpaglione, *Calculation of relaxation functions: A new development within the Mori formalism*, *Physical Review B* **27** (1983) 7342.

[14] O. Bohigas, M.J. Giannoni and C. Schmit, *Characterization of Chaotic Quantum Spectra and Universality of Level Fluctuation Laws*, *Physical Review Letters* **52** (1984) 1.

[15] Y.Y. Atas, E. Bogomolny, O. Giraud and G. Roux, *The distribution of the ratio of consecutive level spacings in random matrix ensembles*, *Physical Review Letters* **110** (2013) 084101 [1212.5611].

[16] F. Haake, S. Gnutzmann and M. Kuś, *Quantum Signatures of Chaos*, Springer Series in Synergetics, Springer International Publishing, Cham (2018), 10.1007/978-3-319-97580-1.

[17] L. D'Alessio, Y. Kafri, A. Polkovnikov and M. Rigol, *From quantum chaos and eigenstate thermalization to statistical mechanics and thermodynamics*, *Advances in Physics* **65** (2016) 239.

[18] T. Mori, T.N. Ikeda, E. Kaminishi and M. Ueda, *Thermalization and prethermalization in isolated quantum systems: A theoretical overview*, *Journal of Physics B: Atomic, Molecular and Optical Physics* **51** (2018) 112001.

[19] J.M. Deutsch, *Quantum statistical mechanics in a closed system*, *Physical Review A* **43** (1991) 2046.

[20] M. Srednicki, *Chaos and quantum thermalization*, *Physical Review E* **50** (1994) 888.

[21] J.M. Deutsch, *Eigenstate Thermalization Hypothesis*, *Reports on Progress in Physics* **81** (2018) 082001 [1805.01616].

[22] E. Brézin and S. Hikami, *Spectral form factor in a random matrix theory*, *Physical Review E* **55** (1997) 4067.

[23] G. Cipolloni, L. Erdős and D. Schröder, *On the Spectral Form Factor for Random Matrices*, *Communications in Mathematical Physics* **401** (2023) 1665.

[24] K. Hashimoto, K. Murata and R. Yoshii, *Out-of-time-order correlators in quantum mechanics*, *Journal of High Energy Physics* **2017** (2017) 138 [1703.09435].

[25] J. Maldacena, S.H. Shenker and D. Stanford, *A bound on chaos*, *Journal of High Energy Physics* **2016** (2016) 106.

[26] D.E. Parker, X. Cao, A. Avdoshkin, T. Scaffidi and E. Altman, *A universal operator growth hypothesis*, *Physical Review X* **9** (2019) .

[27] A. Avdoshkin, A. Dymarsky and M. Smolkin, *Krylov complexity in quantum field theory, and beyond*, *Journal of High Energy Physics* **2024** (2024) 66.

[28] Y. Sekino and L. Susskind, *Fast Scramblers*, *Journal of High Energy Physics* **2008** (2008) 065 [0808.2096].

[29] L. Susskind, *Computational Complexity and Black Hole Horizons*, Feb., 2014. 10.48550/arXiv.1402.5674.

[30] L. Susskind, *Addendum to Computational Complexity and Black Hole Horizons*, Mar., 2014. 10.48550/arXiv.1403.5695.

[31] A. Dymarsky and M. Smolkin, *Krylov complexity in conformal field theory*, *Physical Review D* **104** (2021) L081702.

[32] C. Liu, H. Tang and H. Zhai, *Krylov Complexity in Open Quantum Systems*, *Physical Review Research* **5** (2023) 033085 [2207.13603].

[33] P. Caputa, J.M. Magan and D. Patramanis, *Geometry of Krylov Complexity*, Oct., 2021.

[34] M. Baggioli, K.-B. Huh, H.-S. Jeong, K.-Y. Kim and J.F. Pedraza, *Krylov complexity as an order parameter for quantum chaotic-integrable transitions*, July, 2024. 10.48550/arXiv.2407.17054.

[35] J. Murugan and H. Nastase, *A 4D duality web*, Mar., 2021. 10.48550/arXiv.2103.12667.

[36] J. Murugan and H. Nastase, *A nonabelian particle-vortex duality in gauge theories*, *Journal of High Energy Physics* **2016** (2016) 141.

[37] N. Seiberg, T. Senthil, C. Wang and E. Witten, *A Duality Web in 2+1 Dimensions and Condensed Matter Physics*, June, 2016. 10.1016/j.aop.2016.08.007.

[38] A. Karch and D. Tong, *Particle-Vortex Duality from 3D Bosonization*, *Physical Review X* **6** (2016) 031043.

[39] A. Karch, D. Tong and C. Turner, *A web of 2d dualities: ${\bf Z}_2$ gauge fields and Arf invariants*, *SciPost Physics* **7** (2019) 007.

[40] B.L. Español and D.A. Wisniacki, *Assessing the saturation of Krylov complexity as a measure of chaos*, *Physical Review E* **107** (2023) 024217.

[41] P. Caputa, N. Gupta, S.S. Haque, S. Liu, J. Murugan and H.J.R. Van Zyl, *Spread Complexity and Topological Transitions in the Kitaev Chain*, *Journal of High Energy Physics* **2023** (2023) 120 [2208.06311].

[42] J.D. Noh, *Operator growth in the transverse-field Ising spin chain with integrability-breaking longitudinal field*, *Physical Review E* **104** (2021) 034112.

[43] M. Alishahiha, S. Banerjee and M.J. Vasli, *Krylov Complexity as a Probe for Chaos*, Sept., 2024. 10.48550/arXiv.2408.10194.

[44] A.R. Brown and L. Susskind, *Second law of quantum complexity*, *Physical Review D* **97** (2018) 086015.

[45] A.N. Kolmogorov, *Three approaches to the quantitative definition of information **, *International Journal of Computer Mathematics* **2** (1968) 157.

[46] P.M.B. Vitányi, *How Incomputable Is Kolmogorov Complexity?*, *Entropy* **22** (2020) 408.

[47] F.G. Brandão, W. Chemissany, N. Hunter-Jones, R. Kueng and J. Preskill, *Models of Quantum Complexity Growth*, *PRX Quantum* **2** (2021) 030316.

[48] R. Jefferson and R.C. Myers, *Circuit complexity in quantum field theory*, *Journal of High Energy Physics* **2017** (2017) 107 [1707.08570].

[49] S. Chapman, M.P. Heller, H. Marrochio and F. Pastawski, *Toward a Definition of Complexity for Quantum Field Theory States*, *Physical Review Letters* **120** (2018) 121602.

[50] M.A. Nielsen, M.R. Dowling, M. Gu and A.C. Doherty, *Quantum Computation as Geometry*, *Science* **311** (2006) 1133.

[51] M.A. Nielsen, *A geometric approach to quantum circuit lower bounds*, *Quantum Info. Comput.* **6** (2006) 213.

[52] M.R. Dowling and M.A. Nielsen, *The geometry of quantum computation*, *Quantum Info. Comput.* **8** (2008) 861.

[53] K. Pal, K. Pal and T. Sarkar, *Nielsen complexity of coherent spin state operators*, *Physical Review E* **105** (2022) 064117 [2106.11842].

[54] V. Balasubramanian, P. Caputa, J. Magan and Q. Wu, *Quantum chaos and the complexity of spread of states*, *Physical Review D* **106** (2022) 046007 [2202.06957].

[55] A. Sánchez-Garrido, *On Krylov Complexity*, July, 2024.

[56] S.E. Aguilar-Gutierrez and A. Rolph, *Krylov complexity is not a measure of distance between states or operators*, Nov., 2023.

[57] D.A. Roberts, D. Stanford and A. Streicher, *Operator growth in the SYK model*, *Journal of High Energy Physics* **2018** (2018) 122.

[58] L. Kaplan, *Scars in quantum chaotic wavefunctions*, *Nonlinearity* **12** (1999) R1.

[59] D.A. Roberts, D. Stanford and L. Susskind, *Localized shocks*, *Journal of High Energy Physics* **2015** (2015) 51.

[60] E. Rabinovici, A. Sánchez-Garrido, R. Shir and J. Sonner, *Operator complexity: A journey to the edge of Krylov space*, *Journal of High Energy Physics* **2021** (2021) 62 [2009.01862].

[61] A. Altland and J. Sonner, *Late time physics of holographic quantum chaos*, *SciPost Physics* **11** (2021) 034.

[62] C. Beetar, N. Gupta, S.S. Haque, J. Murugan and H.J.R. Van Zyl, *Complexity and operator growth for quantum systems in dynamic equilibrium*, *Journal of High Energy Physics* **2024** (2024) 156.

[63] E.H. Lieb and D.W. Robinson, *The finite group velocity of quantum spin systems*, *Communications in Mathematical Physics* **28** (1972) 251.

[64] N. Hörnedal, N. Carabba, A.S. Matsoukas-Roubeas and A. del Campo, *Ultimate speed limits to the growth of operator complexity*, *Communications Physics* **5** (2022) 1.

[65] A. Bhattacharya, P.P. Nath and H. Sahu, *Speed limits to the growth of Krylov complexity in open quantum systems*, *Physical Review D* **109** (2024) L121902 [2403.03584].

[66] J.J. Sakurai and J. Napolitano, "Modern Quantum Mechanics." https://www.cambridge.org/highereducation/books/modern-quantum-mechanics/DF43277E8AEDF83CC12EA62887C277DC, Sept., 2020. 10.1017/9781108587280.

[67] J. Schwichtenberg, *Physics from Symmetry*, Undergraduate Lecture Notes in Physics, Springer International Publishing, Cham (2018), 10.1007/978-3-319-66631-0.

[68] M.A. Nielsen, *The Fermionic canonical commutation relations and the Jordan-Wigner transform*, .

[69] P. Jordan and E. Wigner, *Über das Paulische Äquivalenzverbot*, *Zeitschrift für Physik* **47** (1928) 631.

[70] J.W. Negele, *Quantum Many-particle Systems*, CRC Press, Boca Raton (May, 2019), 10.1201/9780429497926.

[71] G.B. Mbeng, A. Russomanno and G.E. Santoro, *The quantum Ising chain for beginners*, Sept., 2020.

[72] A. Dutta, G. Aeppli, B.K. Chakrabarti, U. Divakaran, T.F. Rosenbaum and D. Sen, *Quantum phase transitions in transverse field spin models: From statistical physics to quantum information*, June, 2015.

[73] K. Chhajed, *From Ising model to Kitaev Chain – An introduction to topological phase transitions*, *Resonance* **26** (2021) 1539 [2009.01078].

[74] Z. Weinstein, R. Sajith, E. Altman and S.J. Garratt, *Nonlocality and entanglement in measured critical quantum Ising chains*, *Physical Review B* **107** (2023) 245132.

[75] E. van der Wurff, *Student Seminar on Quantum Integrability - Lecture 4: The Heisenberg XXZ model*, Oct., 2013.

[76] A.N. Kirillov and N.Y. Reshetikhin, *Exact solution of the integrable XXZ Heisenberg model with arbitrary spin. I. The ground state and the excitation spectrum*, *Journal of Physics A: Mathematical and General* **20** (1987) 1565.

[77] S. Tolmay, *Coordinate Bethe Ansatz and Quantum Group Symmetry of the Spin-1/2 XXZ Heisenberg Spin Chain*, Jan., 2015.

[78] M.A. Continentino, *Topological phase transitions*, *Physica B: Condensed Matter* **505** (2017) A1.

[79] S. Huang, *Introduction to Majorana Zero Modes in a Kitaev Chain*, Nov., 2021. 10.48550/arXiv.2111.06703.

[80] H. Pan and S.D. Sarma, *Majorana nanowires, Kitaev chains, and spin models*, *Physical Review B* **107** (2023) 035440 [2208.06108].

[81] X. Chen, Z.-C. Gu and X.-G. Wen, *Classification of Gapped Symmetric Phases in 1D Spin Systems*, *Physical Review B* **83** (2011) 035107 [1008.3745].

[82] X. Chen, Z.-C. Gu and X.-G. Wen, *Complete classification of one-dimensional gapped quantum phases in interacting spin systems*, *Physical Review B* **84** (2011) 235128.

[83] A. Kapustin and R. Thorngren, *Fermionic SPT phases in higher dimensions and bosonization*, *Journal of High Energy Physics* **2017** (2017) 80 [1701.08264].

[84] H.D. Simon, *The Lanczos AlgorithmWith Partial Reorthogonalization*, .

[85] R.M. Larsen, *Lanczos Bidiagonalization With Partial Reorthogonalization*, *DAIMI Report Series* (1998) .

[86] D.C. Sorensen, *Implicit Application of Polynomial Filters in a k-Step Arnoldi Method*, *SIAM Journal on Matrix Analysis and Applications* **13** (1992) 357.

[87] R.B. Lehoucq and D.C. Sorensen, *Deflation Techniques for an Implicitly Restarted Arnoldi Iteration*, *SIAM Journal on Matrix Analysis and Applications* **17** (1996) 789.

[88] E. Rabinovici, A. Sánchez-Garrido, R. Shir and J. Sonner, *Krylov localization and suppression of complexity*, *Journal of High Energy Physics* **2022** (2022) .

[89] K. Hashimoto, K. Murata, N. Tanahashi and R. Watanabe, *Krylov complexity and chaos in quantum mechanics*, *Journal of High Energy Physics* **2023** (2023) .

[90] K. Kawabata, R. Kobayashi, N. Wu and H. Katsura, *Exact zero modes in twisted Kitaev chains*, *Physical Review B* **95** (2017) 195140.

[91] J.M. Magan and J. Simon, *On operator growth and emergent poincaré symmetries*, *Journal of High Energy Physics* **2020** (2020) 71 [2002.03865].